

Local energy of a bubble system and its loss due to acoustic radiation

Wang, Qian

DOI:
[10.1017/jfm.2016.281](https://doi.org/10.1017/jfm.2016.281)

License:
Creative Commons: Attribution-NonCommercial-NoDerivs (CC BY-NC-ND)

Document Version
Peer reviewed version

Citation for published version (Harvard):
Wang, Q 2016, 'Local energy of a bubble system and its loss due to acoustic radiation', *Journal of Fluid Mechanics*, vol. 797, pp. 201-230. <https://doi.org/10.1017/jfm.2016.281>

[Link to publication on Research at Birmingham portal](#)

General rights

Unless a licence is specified above, all rights (including copyright and moral rights) in this document are retained by the authors and/or the copyright holders. The express permission of the copyright holder must be obtained for any use of this material other than for purposes permitted by law.

- Users may freely distribute the URL that is used to identify this publication.
- Users may download and/or print one copy of the publication from the University of Birmingham research portal for the purpose of private study or non-commercial research.
- User may use extracts from the document in line with the concept of 'fair dealing' under the Copyright, Designs and Patents Act 1988 (?)
- Users may not further distribute the material nor use it for the purposes of commercial gain.

Where a licence is displayed above, please note the terms and conditions of the licence govern your use of this document.

When citing, please reference the published version.

Take down policy

While the University of Birmingham exercises care and attention in making items available there are rare occasions when an item has been uploaded in error or has been deemed to be commercially or otherwise sensitive.

If you believe that this is the case for this document, please contact UBIRA@lists.bham.ac.uk providing details and we will remove access to the work immediately and investigate.

Local energy of a bubble system and its loss due to acoustic radiation

Q. X. Wang* (Qianxi Wang)

School of Mathematics, the University of Birmingham,
Ring Rd N, Birmingham B15 2TS, United Kingdom

Energy concentration and loss due to a violent collapsing bubble are essential phenomena to many applications such as cavitation erosion, biomedical ultrasonics, sonochemistry, cavitation cleaning and underwater explosions. It has been generally known that the energy of a bubble system is radiated away as an acoustic wave and dissipated by viscosity. However, there is no study in the scientific literature on the time history of the energy of a bubble system in a compressible flow. Here we have introduced the local energy of a nonspherical bubble system, consisting of the energy of the interior gas, the interface and the exterior liquid in the inner asymptotic region. The local energy determines the local bubble and flow dynamics, including the concentration of energy, stress and momentum. We obtain a simple formula for the radiated energy associated with acoustic radiation in terms of the bubble volume history. We perform calculations of the energy history for a transient bubble in a compressible liquid, in an infinite fluid, subject to buoyancy and near a rigid boundary, respectively. Our calculations show that the local energy of a transient bubble follows a step function in time, being nearly conserved for most of each cycle of oscillation but decreasing rapidly and significantly at bubble inception and at the end of collapse, due to the emission of steep pressure waves or shock waves. The loss of the local energy of the bubble system due to emission of steep pressure waves and the associated damping of the bubble oscillation are diminished by buoyancy effects and decrease with the buoyancy parameter. Similarly, the loss of the local energy of a bubble system is diminished by the presence of a rigid boundary and decreases with the proximity of the bubble to the boundary. We also analyse the energy concentration of single bubble sonoluminescence in a standing acoustic wave.

Keywords: Local energy of a bubble system; Acoustic radiation; Shock waves; Bubble dynamics; Sonoluminescence; Weakly compressible theory; Matched asymptotic expansions; Boundary integral method.

* Email address for correspondence: q.x.wang@bham.ac.uk or wqianxi@yahoo.com

1. Introduction

Cavitation was discovered in 1893 from the propeller failure of a British warship (Young 1989). While a cavitation bubble collapses, its volume often reduces by a factor of several thousand, leading to a high concentration of energy, and associated emission of shock waves and high-speed liquid jetting. These phenomena are associated with cavitation damage to pumps, turbines and propellers (Brennen 1995; Lauterborn & Vogel 2013), and the damage mechanism of an underwater explosion (Cole 1948, Chahine et al. 1980, Klaseboer et al. 2005).

Ultrasound-driven microbubbles have been used in extracorporeal shockwave lithotripsy (Calvisi et al. 2008), tissue ablation (Roberts et al. 2006), oncology and cardiology (Leslie et al. 2006), and sonoporation – a new, promising cell-wall permeation technique (Coussios & Roy 2007, Wang et al. 2015). In these applications, microbubbles absorb and concentrate significant amounts of acoustic energy into a small volume, leading to violent collapse, emission of shock waves and the formation of liquid jets (Wang & Manmi 2014). These mechanisms are also common to sonochemistry (Suslick 1990) and ultrasonic cavitation cleaning (Ohl 2006).

The energy of a bubble system is thus a basic and important concept for bubble dynamics and its applications. A bubble system consists of the exterior liquid extending to infinity, the gases inside the bubble and the interface between them. Its initial energy is created by various means, depending on how the bubble is produced. For example, the initial energy is deposited by a laser beam for laser-generated bubbles, by explosion for underwater explosion bubbles, and by the work done by highly compressed gases for seismic airgun-generated bubbles, etc.

Cole (1948) suggested the following regarding energy loss for a bubble system, ‘... the mechanism by which energy can be dissipated: the compressibility of the water, by which energy is radiated as a wave and ultimately dissipated as heat as the wave passes to infinite distance, ...’. This energy loss mechanism has been confirmed by numerous experiments on bubble dynamics displaying the emission of steep pressure waves at bubble inception and at the end of collapse, and damped bubble oscillation due to loss of energy (Lauterborn & Vogel 2013). The acoustic waves emitted at the inception of a bubble and at the end of collapse exhibit steepening feature in the pressure profile due to nonlinearity, which are termed as shock waves in literature (c.f. Plesset & Prosperetti 1977; Philipp & Lauterborn 1998; Geers et al. 2012; Tinguely et al. 2012; Lauterborn & Vogel 2013).

The mechanical energy of a bubble system consists of the potential energy and kinetic energy. When the liquid flow is incompressible and potential, its kinetic energy can be expressed in terms of an integral over the bubble surface (Cole 1948; Pearson et al. 2004). To account for the emission of acoustic waves, the liquid flow has to be modelled as compressible. The calculation of the kinetic energy in this case thus involves volume integration of the density and velocity of the liquid flow

throughout the entire flow field.

Geers et al. (2012) and Tinguely et al. (2012) studied the energy of a spherical bubble, with the bubble radius history calculated using the Keller–Miksis equation (Keller & Kolodner 1956, Keller & Miksis 1980, Feng & Leal 1997). They introduced the inviscid flow assumption, so that the radiated energy during the end of collapse is equal to the energy difference of the bubble system between the first and second maximum volumes, based on conservation of energy. With that, they calculated the radiated energy during the end of collapse. This approach avoids the calculation of the kinetic energy in a compressible flow. However, it cannot be used to calculate the energy loss associated with the emission of steep waves at bubble inception and cannot be used when viscosity is not negligible.

There is no study in the scientific literature on the time history of the energy of a bubble system in a compressible flow, showing how and when the energy is lost. The bubble energy for nonspherical bubbles is calculated only during the period when the compressible effects are negligible and the energy loss is obtained from experiments and empirical formulae (Lee et al. 2007). In this work, we calculate the time history of a bubble system in a compressible flow, considering compressibility of the exterior liquid for both spherical and nonspherical bubbles, and viscosity of the flow for spherical bubbles. The mechanical energy lost due to thermal conductivity is not considered in this paper.

We introduce the local energy of a bubble system consisting of the potential energy and kinetic energy of the liquid flow in the inner region. The local kinetic energy can be calculated approximately using an incompressible model, since the flow in the inner region is approximately incompressible to second order (Prosperetti & Lezzi 1986, Lezzi & Prosperetti 1987, Wang & Blake 2010, 2011).

For spherical bubbles, this paper builds on the developments of Geers et al. (2012) and Tinguely et al. (2012) by considering the following: (i) calculation of the time history of the local bubble energy, which indicates when and how fast the local energy is lost, (ii) analysis of the local energy loss associated with the emission of a steep pressure wave at bubble inception, which is significant for transient bubbles, (iii) the energy loss due to viscous effects, which is essential for microbubbles, (iv) surface tension effects, which are also essential for microbubbles, and (v) the influence of acoustic waves.

For nonspherical bubbles, we present the calculation of the time history of the energy of a bubble system in a compressible flow for two cases: (i) A gas bubble subject to buoyancy, and (ii) a cavitation bubble near a rigid boundary. The weakly compressible potential flow is modelled here using a recently developed implementation of the boundary integral method (BIM) for a bubble in a compressible liquid (Wang & Blake 2010, 2011, Wang 2013, 2014). By the way, nonspherical

bubble dynamics in a compressible liquid have been simulated using domain approaches coupled with various interface-capturing schemes (Johnsen & Colonius 2006, 2008, 2009, Turangan et al. 2008, Terashima et al. 2009, Fuster et al. 2011, Hiao et al. 2014, Chahine et al. 2015, 2016).

This paper is organized as follows. In §2, the flow problem is formulated based on the weakly compressible potential flow theory. In §3, we derived the formulae for the local energy of a nonspherical bubble system, consisting of the energy of the interior gas, the interface and the exterior liquid in the inner region. We obtain a simple formula for the radiated energy, in terms of the bubble volume history. The time history of energy of a spherical transient bubble is analysed in §4, based on the Keller–Miksis equation. The energy history of nonspherical transient bubbles subject to buoyancy and near a rigid boundary are analysed in §5 and §6 respectively, using the compressible BIM model. It is noted that the energy of a bubble system follows a step function in time, reducing significantly at bubble inception and at the end of collapse, while remaining nearly constant during the remainder of the oscillation. We analyse the energy loss in terms of the buoyancy parameter and the standoff distance of a bubble from a rigid boundary. In §7, the energy concentration of single bubble sonoluminescence is studied, using the Keller–Miksis equation. Finally, in §8, this study is summarized and the key outcomes are identified.

2. Weakly compressible theory

Consider gas bubble dynamics in an irrotational and compressible liquid flow. A Cartesian-coordinate system is chosen, with the origin at the centre of the bubble at inception, and the z -axis in the direction opposite of gravity.

The reference length is chose as the maximum bubble radius R_{\max} that a bubble would expand to in an inviscid liquid and without surface tension effects. The density ρ_{∞} in the undisturbed liquid is chosen as the reference density. The reference pressure is $\Delta p = p_{\infty} - p_v$, where p_{∞} is the pressure in the undisturbed liquid and p_v is the partial pressure of vapour inside the bubble. The vapour pressure p_v is approximately a function of the temperature of the bubble wall only, if the time scale of condensation and evaporation is small compared to the period of bubble oscillation. It is usually small ($p_v \sim 2$ kPa at 20°C) compared to the hydrostatic pressure and is often negligible (Brennen 1995). The reference velocity is thus obtained as $U = \sqrt{\Delta p / \rho_{\infty}}$. We introduce dimensionless quantities, denoted by subscripts “*”, as follows:

$$\mathbf{r}_* = \frac{\mathbf{r}}{R_{\max}}, \quad t_* = \frac{U}{R_{\max}} t, \quad \varphi_* = \frac{\varphi}{R_{\max} U}, \quad (2.1a, b, c)$$

$$c_* = \frac{c}{c_{\infty}}, \quad p_* = \frac{p - p_{\infty}}{\Delta p}, \quad (2.1d, e)$$

where $\mathbf{r} = (x, y, z)$, t is the time, ϕ is the velocity potential of the liquid flow and p is the pressure. The speed of sound c is normalized by its value in the undisturbed liquid c_∞ .

The highest speed of the liquid flow induced by bubble dynamics is usually associated with the velocity of the bubble jet, which is often lower than 200 m s^{-1} at normal ambient pressure, as observed in experiments (Benjamin & Ellis 1966, Lauterborn & Bolle 1975, Shima et al. 1981, Tomita & Shima 1986, Vogel et al. 1989, 1990, Lauterborn & Ohl 1997, Philipp & Lauterborn 1998, Lindau, & Lauterborn 2003, Brujan & Matsumoto 2012, Yang et al. 2013; Zhang et al. 2015). As the speed of sound in water is about 1500 m s^{-1} , the flow induced by the bubble dynamics is assumed to be associated with a low Mach number, ε , defined as follows:

$$\varepsilon = \frac{U}{c_\infty}. \quad (2.2)$$

Lauterborn & Vogel (2013) observed that the newly formed laser bubble's surface expands with an initial velocity of about 2450 ms^{-1} , which decays rapidly to about 250 ms^{-1} within 140 ns . The present model is only valid after that. Note that the term ‘‘bubble inception’’ used in the paper refers to the moment during the early stage of expansion, when the bubble wall Mach number starts being small.

We divide the fluid domain into two regions: the inner region near the bubble where $(x, y, z) = O(R_{\max})$ and the outer region far away from the bubble where $(x, y, z) = O(\lambda)$, where $\lambda = c_\infty R_{\max}/U$ is the wavelength of acoustic waves.

Using the method of matched asymptotic expansions, the outer solution was shown to satisfy the wave equation to second order and was found analytically as follows (Wang 2013, 2014):

$$\phi_{outer} = \varepsilon C_0 \frac{m_0(t_* - \tilde{r})}{\tilde{r}} + O(\varepsilon^2), \quad (2.3)$$

where $\tilde{r} = r/\lambda = \varepsilon r_*$, $r = |\mathbf{r}|$, and C_0 is a given constant with a value of $1/(4\pi)$ and $1/(2\pi)$ for a bubble in an unbounded liquid and near a rigid boundary, respectively. The quantity $m_0(t_*)$ is obtained from matching the inner and outer expansions using Van Dyke's matching principle (Van Dyke 1975, Wang 2013, 2014) as follows:

$$m_0(t_*) = \int_S \frac{\partial \phi(\mathbf{q}, t_*)}{\partial n} dS(\mathbf{q}) = -\dot{V}_*(t_*), \quad (2.4)$$

where \mathbf{n} is the unit normal vector on the bubble surface and the overdot denotes the derivative with respect to time.

The inner solution to second order satisfies Laplace's equation and the kinematic and dynamic boundary conditions on the bubble surface, S , as follows (Wang & Blake 2010):

$$\nabla_*^2 \phi_* = O(\varepsilon^2), \quad (2.5a)$$

$$\frac{D\mathbf{r}_*}{Dt_*} = \nabla_* \varphi_* + O(\varepsilon^2) \quad \text{on } S, \quad (2.5b)$$

$$\frac{D\varphi_*}{Dt_*} = 1 + \frac{1}{2} |\nabla_* \varphi_*|^2 - p_{L*} - \delta^2 z_* + O(\varepsilon^2) \quad \text{on } S, \quad (2.5c)$$

where $\delta = \sqrt{\rho g R_m / \Delta p}$ is the buoyancy parameter, where g is the gravitational acceleration. The liquid pressure, p_L , on the bubble surface is given by,

$$p_{L*} = p_{B*} - \sigma_* \nabla \cdot \mathbf{n} \quad \text{on } S, \quad (2.6a)$$

$$p_{B*} = p_{v*} + p_{g0*} \left(\frac{V_{0*}}{V_*} \right)^\kappa, \quad (2.6b)$$

where p_{B*} is the pressure of the bubble contents, $p_{g0*} = p_{g0}/\Delta p$ is the initial partial pressure of the non-condensable gases inside the bubble, V_{0*} is the initial bubble volume, κ is the polytropic index of the bubble gas, $\nabla \cdot \mathbf{n}$ provides the surface curvature and $\sigma_* = \sigma/(R_m \Delta p)$ is the surface tension parameter. Here variables with the subscript of “*” are dimensionless. We assumed in (2.6) that the expansion and contraction of the bubble gases occur adiabatically. We will not consider the thermal effects associated with this phenomenon, which can lead to chemical reactions (Suslick 1990) and sonoluminescence (Hiller et al. 1998, Hilgenfeldt et al. 1998, 1999). Fuster & Montel (2015) showed that for very fast oscillations the effective polytropic coefficient of the mixture recovers the adiabatic limit given that neither heat nor mass transfer has time significantly modify the pressure inside the bubble. The thermal processes typically absorb a relatively small portion of the overall energy (Akhatov et al. 2001). Heat and mass transfer across the bubble surface can be included in the model (Szeri et al. 2003).

We also assume in (2.6) that the pressure field in the bubble interior is uniform, since the density of gases is usually three orders of magnitude smaller than that of liquids. Geers et al. (1994, 2002, 2012) employed the doubly asymptotic approximations for spherical bubble dynamics for both the external liquid and the internal gases. They noticed that while acoustic-wave effects in the external liquid are important, such effects in the internal gases are not.

The far field boundary condition of the inner solution is obtained by matching with the outer solution as follows:

$$\varphi_* \rightarrow C_0 \left(\varepsilon \ddot{V}_*(t_*) - \frac{\dot{V}_*(t_*)}{r_*} \right) + O(\varepsilon^2) \quad \text{as } r_* \rightarrow \infty. \quad (2.5d)$$

The initial condition on the boundary is given as

$$\varphi_{n*}|_{t_*=0} = -R_{t0*} \quad \text{on } r_* = R_{0*}, \quad (2.5e)$$

where R_{0*} and R_{t0*} are the initial radius of the bubble and the initial rate of change of the bubble radius, respectively.

Examining the initial and boundary value problem of (2.5), one can see that the compressible effects to second order appear only in the far field condition (2.5d). As the basic equation is Laplace's equation, this problem can be modeled using the boundary integral method (BIM). The details on the numerical model using the BIM for this problem can be found in (Wang et al. 1996a, Curtiss et al. 2013).

A nonspherical bubble collapse often leads to the formation of a high speed liquid jet. The jet subsequently impacts the opposite bubble surface and penetrates the bubble, and the liquid domain is then transformed from a singly connected to a doubly connected domain. The solution to a potential problem in a doubly connected domain is non-unique. The doubly connected domain can be made singly connected by, for example, using a branch cut by Best (1993) or a vortex sheet by Zhang, Duncan & Chahine (1993) and Zhang & Duncan (1994).

Pedley (1968) and Lundgren & Mansour (1991) modeled the dynamics of a bubble torus with a vortex ring inside, started with a circular cross-section. Wang, et al. (1996b, 2005) developed a vortex ring model from these earlier ideas to model the topological transition of a singly connected bubble to a subsequent toroidal bubble. In the vortex ring model, a vortex ring is put inside the toroidal bubble after jet impact. The circulation of the vortex ring is equal to the jump of the potential φ_* across the contact point at the time of jet impact

$$\Gamma_* = \oint_C \nabla_* \varphi_* \cdot d\mathbf{r} = \varphi_{N*} - \varphi_{S*}, \quad (2.7)$$

where φ_{N*} and φ_{S*} are potentials at the impact point. Here we assume jet impact occurs at a single point. The potential φ_* is then decomposed as follows:

$$\varphi_* = \varphi_{vr} + \phi, \quad (2.8)$$

where φ_{vr} is the potential of the vortex ring, which can be obtained from the Biot-Savart law. With the potential jump being accounted for by the vortex ring using (2.8), the remnant potential ϕ is continuous in the flow field and can be simulated using the BIM model (Wang 2005).

Zhang et al. (1993) considered the loss of the mechanical energy due to jet impact and obtained a formula for the energy loss, which exists when the impact occurs over a finite area. Rogers et al. (1990) and Szymczak et al. (1993) also noted an energy loss during impact and presented a similar formula. Jet impact often happens on a small area, since the curvature radius of the jet front is usually smaller than the curvature radius of the opposite bubble wall at the location of impact. Important energy conversions following jet impact and jet penetration through the bubble, which may result in bubble mass loss, formation of numerous satellites microbubbles and bubble fission, and formation of bubble clouds. Although jet impact may be more complex in reality, we assume in this paper that jet impact occurs at a point, an idealized model, and do not calculate the loss and conversion of energy due to jet impact.

3. Local energy of a bubble system in a compressible liquid

This paper is concerned only with the mechanical energy of a bubble system, not considering for heat transfer, evaporation or condensation, etc. The total mechanical energy E_T of a bubble system consists of the local energy E_L within the inner region and the acoustic radiation energy E_A radiated outside of the inner region, i.e.

$$E_T = E_L + E_A. \quad (3.1)$$

It is natural to separate the mechanical energy of a bubble system into the local energy and acoustic radiation energy, since different length/time scales of decay are associated with the incompressible fluid motion and the acoustic radiation associated with the bubble dynamics.

For a bubble system in a compressible liquid, the inner region Ω_L is bounded by the bubble surface S and a large sphere S_L , with its centre at the centre of the initial bubble surface and a radius R_L , as shown in figure 1a. R_L is much larger than the maximum bubble radius R_{\max} but much smaller than the wavelength λ : $R_{\max} \ll R_L \ll \lambda$. The local mechanical energy E_L of a bubble system consists of the local potential energy E_{LP} and the local kinetic energy E_{LK} within S_L .

For a bubble near a flat rigid boundary, it is equivalent to the interaction of the bubble and its image to the boundary, as illustrated in figure 1b. The inner region is then bounded by the bubble surface S , its image, and a large sphere S_L , with its centre at the centre of the two bubble surfaces at inception and the radius R_L .

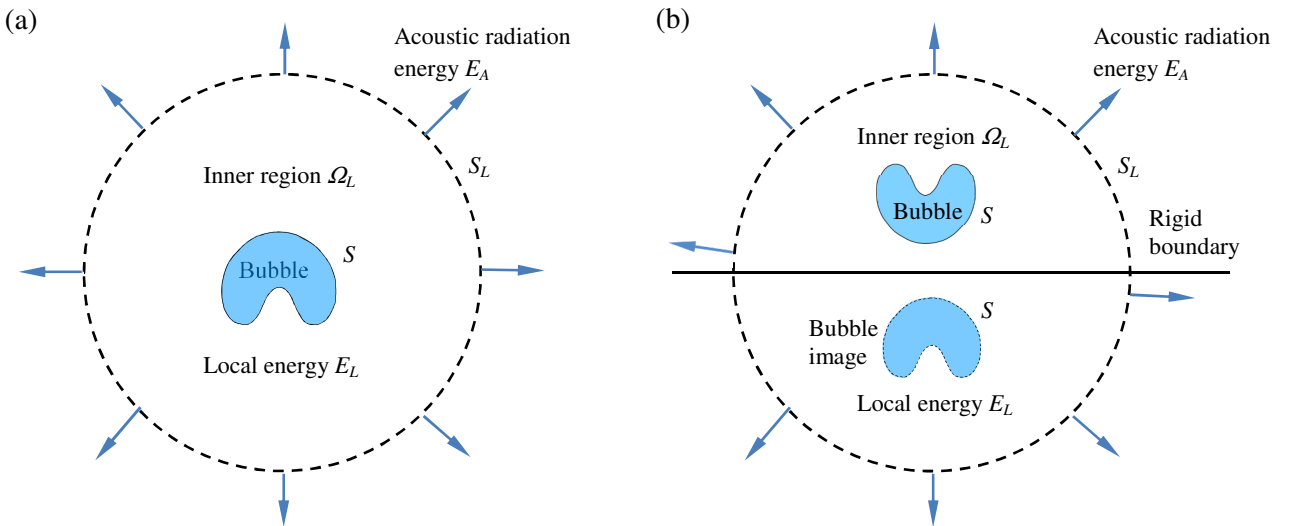


Figure 1. (a) Illustration of the inner region Ω_L of the flow field for a bubble in an infinite domain bounded by the bubble surface S and a large sphere S_L , with its centre at the centre of the initial bubble surface and with a radius R_L satisfying $R_{\max} \ll R_L \ll \lambda$, where R_{\max} and λ are the maximum equivalent bubble radius and the wavelength of acoustic waves, respectively. The total mechanical energy E_T of a bubble system consists of the local energy E_L within the inner region and the acoustic radiation energy E_A radiated outside of the inner region. (b) Illustration of the inner region Ω_L of the flow field for a bubble near a rigid flat boundary.

3.1 Local potential energy of a bubble system

Potential energy is energy a system has by virtue of its state or configuration. The potential energy at a particular state is the work required to move the system from a state of zero potential energy to the state required. The potential energy does not depend on the process to achieve the state. We set the potential energy as zero initially, since it can be added with an arbitrary constant. The potential energy can thus be calculated using an idealised and infinitely slow process, so that no energy is converted to kinetic energy, radiated far away due to acoustic waves or lost due to viscous effects or heat transfer, etc. In this way, all the work done is turned into potential energy. Potential energy is thus the same whether a bubble is in an incompressible liquid or a compressible liquid, since it does not depend on the compressible effects of the liquid.

As a bubble expands or collapses infinitely slowly and adiabatically from its initial shape to its present shape, the local potential energy is equal to the sum of (i) the work done on the liquid by the gas pressure at the bubble wall and (ii) the power transmitted across S_L , i.e.

$$E_{LP} = -\int_{V_0}^V p_B dV + p_\infty (V - V_0) - \rho g V z_c, \quad (3.2)$$

where the first two terms on the right hand side correspond to (i) and (ii) described above, respectively. The power transmitted across S_L is calculated based on two facts: the pressure at S_L is equal to p_∞ to first order and the volume flux of the flow through S_L is the same as the change of the bubble volume because the flow is incompressible to second order in the inner region. The third term is the work done to move the bubble infinitely slowly from its centre position at $z = 0$ to $z = z_c$ against gravity, where the z -axis is in the direction opposite gravity.

Substituting (2.6) into (3.2) yields

$$\begin{aligned} E_{LP} &= -\int_{V_0}^V \left(p_v + p_{g0} \left(\frac{V_0}{V} \right)^\kappa - \sigma \nabla \cdot \mathbf{n} \right) dV + p_\infty (V - V_0) - \rho g V z_c \\ &= (p_\infty - p_v)(V - V_0) + \frac{p_{g0} V_0}{\kappa - 1} \left(\left(\frac{V_0}{V} \right)^{\kappa-1} - 1 \right) + \sigma \left(\oint_{S_b} \mathbf{n} \cdot \mathbf{n} dS - \oint_{S_{b0}} \mathbf{n} \cdot \mathbf{n} dS \right) - \rho g V z_c \\ &= (p_\infty - p_v)(V - V_0) + \frac{p_{g0} V_0}{\kappa - 1} \left(\left(\frac{V_0}{V} \right)^{\kappa-1} - 1 \right) + \sigma (A - A_0) - \rho g V z_c, \end{aligned} \quad (3.3a)$$

where A_0 and A are the areas of the initial and current bubble surfaces. In (3.3a), the Gauss divergence theorem was used for the term associated with surface tension. The definition of the local potential energy (3.3a) is the same as the potential energy for the incompressible theory (Blake 1988; Zhang et al. 2001; Lee et al. 2007; Pearson et al. 2004). The potential can be modified with the addition of an arbitrary constant and thus can be written as follows:

$$E_{LP} = (p_\infty - p_v)(V - V_0) + \frac{p_{g0}V_0}{\kappa - 1} \left(\frac{V_0}{V} \right)^{\kappa-1} + \sigma A - \rho g V z_c. \quad (3.3b)$$

To study the energy concentration, we introduce the potential energy E_{PG} of the bubble gas, which is equal to the work done to the gas while the bubble expands or collapses infinitely slowly and adiabatically from its initial volume V_0 to the current volume V ,

$$E_{PG} = - \int_{V_0}^V p_{g0} \left(\frac{V_0}{V} \right)^\kappa dV = \frac{p_{g0}V_0}{\kappa - 1} \left(\left(\frac{V_0}{V} \right)^{\kappa-1} - 1 \right). \quad (3.4)$$

E_{PG} increases as the bubble volume decreases and achieves a maximum value when the bubble is at its minimum volume.

3.2 Local kinetic energy of a bubble system

The kinetic energy is mainly contributed from the liquid flow induced by bubble motion, since the density of gases is usually three orders of magnitude smaller than that of liquids. The local kinetic energy E_{LK} of the liquid flow in the inner region is given as follows by using Green's divergence theorem:

$$E_{LK} = \frac{1}{2} \int_{\Omega_L} \rho_* |\nabla_* \varphi_*|^2 dV = \frac{1}{2} \oint_{S+S_L} \varphi_* \frac{\partial \varphi_*}{\partial n} dS + O(\varepsilon^2) = \frac{1}{2} \oint_S \varphi_* \varphi_{n*} dS + O(\varepsilon), \quad (3.5)$$

since it is easy to verify that $\oint_{S_L} \varphi_* \varphi_{n*} dS = C_0^2 4\pi R_{L*}^2 \left(\varepsilon \ddot{V}_*(t_*) - \frac{\dot{V}_*(t_*)}{R_{L*}} \right) \frac{\dot{V}_*(t_*)}{R_{L*}^2} = O(\varepsilon)$, using the outer

limit of the inner solution (2.5d) and $\varphi_{n*}|_{S_L} = \frac{\partial \varphi_{n*}}{\partial r_*} \Big|_{r_*=R_L} = C_0 \frac{\dot{V}_*(t_*)}{R_{L*}^2} + O(\varepsilon^2)$.

The local energy of a bubble system in a compressible liquid consists of the local potential energy E_{LP} and the local kinetic energy E_{LK} as follows:

$$E_L = E_{LP} + E_{LK} = \frac{p_{g0}V_0}{\kappa - 1} \left(\frac{V_0}{V} \right)^{\kappa-1} + \sigma A - \rho g V z_c + (p_\infty - p_v)V + \frac{1}{2} \rho_\infty \oint_S \varphi \varphi_n dS, \quad (3.6)$$

which is the same as the energy of a bubble system in an incompressible liquid. In dimensionless form this yields,

$$E_{L*} = \frac{p_{g0*}V_{0*}}{\kappa - 1} \left(\frac{V_{0*}}{V_*} \right)^{\kappa-1} + \sigma_* A_* + (1 - \delta^2 z_{c*}) V_* + \frac{1}{2} \oint_S \varphi_* \varphi_{n*} dS + O(\varepsilon), \quad (3.7)$$

where $E_{L*} = E_L / (R_m^3 \Delta p)$.

The local energy of a bubble system in a compressible liquid depends on the bubble shape and the potential and normal velocity distributions on the bubble surface. When the flow is not induced by a bubble alone and the environmental flow has a large length scale compared to the bubble radius,

the local energy can be calculated using (3.6). In this case, the potential φ and normal velocity φ_n on the bubble surface can be obtained by considering its flow environment. As an example, we will consider a bubble oscillating in a standing wave in §7.

For the case of spherical bubbles, the formula for the local energy is simplified as

$$E_L = \frac{p_{g0} V_0}{\kappa - 1} \left(\frac{V_0}{V} \right)^{\kappa-1} + \sigma A - \rho g V z_c + (p_\infty - p_v) V + 2\pi \rho_\infty R^3 \dot{R}^2. \quad (3.8)$$

3.3 Acoustic radiation energy

The energy flux N_{flux*} across S_∞ to the far field is given as

$$N_{flux*} = \oint_{S_L} \left(p_* + \frac{1}{2} |\nabla_* \varphi_*|^2 \right) \varphi_{n*} dS = - \oint_{S_L} \frac{\partial \varphi_*}{\partial t_*} \varphi_{n*} dS + O(\varepsilon^2) = -\varepsilon C_0 \dot{V}_*(t_*) \ddot{V}_*(t_*) + O(\varepsilon^2), \quad (3.9)$$

where we used the outer limit of the inner solution (2.5d). There is a first-order energy flux to the far field, corresponding to acoustic radiation. Notice here $E_{L*} = O(1)$ and $N_{flux*} = O(\varepsilon)$, are both obtained to the leading order approximation in (3.7) and (3.9), respectively.

The energy radiated E_A across S_∞ from the start to the current time is given as

$$\begin{aligned} E_{A*} &= \int_0^{t_*} N_{flux*}(t_*) dt_* = -\varepsilon C_0 \int_0^{t_*} \dot{V}_*(t_*) \ddot{V}_*(t_*) dt_* + O(\varepsilon^2) \\ &= \varepsilon C_0 \left\{ \dot{V}_*(0) \ddot{V}_*(0) - \dot{V}_*(t_*) \ddot{V}_*(t_*) + \int_0^{t_*} \ddot{V}_*^2(t_*) dt_* \right\} + O(\varepsilon^2). \end{aligned} \quad (3.10)$$

The formulae in dimensional form are

$$N_{flux} = -C_0 \frac{\rho_\infty}{c_\infty} \dot{V}(t) \ddot{V}(t) + O(\varepsilon^2), \quad (3.11a)$$

$$E_A = C_0 \frac{\rho_\infty}{c_\infty} \left\{ \dot{V}(0) \ddot{V}(0) - \dot{V}(t) \ddot{V}(t) + \int_0^t \ddot{V}^2(t) dt \right\} + O(\varepsilon^2). \quad (3.11b)$$

The radiation energy due to acoustic waves depends only on the bubble volume history to a first order approximation.

In particular, the energy loss due to acoustic radiation from the time at one of the bubble's maximum volumes to the time at the next maximum volume is given as

$$\Delta E_A = C_0 \frac{\rho_\infty}{c_\infty} \int_{t_N}^{t_{N+1}} \ddot{V}^2(t) dt + O(\varepsilon^2), \quad (3.12)$$

where t_N and t_{N+1} are the times of the two successive maximum bubble volumes. As expected, ΔE_A is always positive, since the local energy of a bubble system is always lost through acoustic radiation. The energy loss depends largely on the acceleration of the bubble volume, which achieves maximum values at minimum bubble volumes.

Longuet-Higgins (1989a, b) studied the radiated energy due to a spherical bubble under harmonic oscillation with small amplitude, i.e.

$$R(t) = a(1 + \alpha \sin(\omega t)), \quad \alpha \ll 1, \quad (3.13)$$

where a and $R(t)$ are the equilibrium and transient radii of the bubble, respectively, and ω is the angular frequency of the oscillation. He obtained the average flux over a period of oscillation as follows (eq. (5.2), Longuet-Higgins 1989b), after converting to the current notations:

$$\bar{N}_{flux} = 2\pi \frac{\rho}{c} \alpha^2 \omega^4 a^6. \quad (3.14)$$

Note that ρ is missing from eq. (5.2) in Longuet-Higgins (1989 b), which should be included.

Using (3.13), the rate of the bubble volume can be given as

$$\dot{V} = -4\pi\alpha\omega a^3 \cos(\omega t), \quad \ddot{V} = 4\pi\alpha\omega^3 a^3 \cos(\omega t). \quad (3.15)$$

Substituting (3.15) into (3.11a) yields

$$N_{flux} = 4\pi \frac{\rho}{c} \alpha^2 \omega^4 a^6 \cos^2(\omega t). \quad (3.16)$$

Its average value over a period of oscillation is the same as (3.14). Note that the range of applicability of the expression used in the paper is restricted to strong nonlinear regimes.

3.4 Considerations for introducing the local energy of a bubble system

The local energy is introduced based on the following considerations. The total mechanical energy of a bubble system does not change due to acoustic radiation. When viscous effects are negligible, the total mechanical energy of a bubble system remains constant.

In contrast, the local energy of a bubble system is lost as the acoustic wave energy is radiated irreversibly to the far field. The bubble system with the remaining local energy undergoes damped oscillation with both the amplitude and period reducing significantly. It is the local energy at the time considered, not the total energy, that determines (i) bubble behaviour, and (ii) the forces, stresses, momentum and heat generated by the bubble.

In addition, our computations in §4, §5 and §6 show that the local energy of a transient bubble follows a step function in time, being conserved approximately for most of each oscillation cycle, but decreasing rapidly and significantly at bubble inception and at the end of collapse, due to acoustic radiation. The compressible results are significant only during very short periods at the minimum bubble volumes associated with emission of steep pressure waves. This justifies the hybrid modelling widely used for bubble dynamics: emission of steep pressure waves at inception of a bubble is modelled using a compressible model and subsequent bubble dynamics are modelled using an incompressible model. The hybrid method was developed to study bubble dynamics with emission of a shock wave at the end of collapse by Hsiao et al. (2014).

4. A spherical bubble system

Dynamics of a spherical bubble dynamics in a compressible liquid can be described approximately by the Keller–Miksis equation,

$$(1 - \varepsilon \dot{R}_*) R_* \ddot{R}_* + \frac{3}{2} \dot{R}_*^2 \left(1 - \frac{\varepsilon}{3} \dot{R}_* \right) = p_{L*} + \varepsilon \frac{d(R_* p_{L*})}{dt} + O(\varepsilon^2), \quad (4.1)$$

where

$$p_{L*} = p_{g0*} \left(\frac{R_{0*}}{R_*} \right)^{3\kappa} - 1 - \frac{2\sigma_*}{R_*} - \frac{4}{Re} \frac{\dot{R}_*}{R_*} - p_{a*}(t_*), \quad (4.2)$$

where $p_{a*}(t_*)$ is the acoustic pressure at the location of the centre of the initial bubble, and $Re = \rho_\infty U R_{max} / \mu$ is the Reynolds number, with μ being viscosity. Geers et al. (1994, 2002, 2012) compared the Keller–Miksis equation with the numerical solution of the Euler equation for spherical bubbles for large parameter ranges. They noticed that weakly compressible theory provides very accurate results.

The Keller–Miksis equation is integrated using the fourth order Runge-Kutta method, to obtain $R(t)$, $\dot{R}(t)$ and $\ddot{R}(t)$ and $V(t)$, $\dot{V}(t)$ and $\ddot{V}(t)$. With that, the energy flux N_{flux} and the radiated energy E_A to the far field can be calculated using (3.11). The calculations were performed for relative and absolute tolerances being 10^{-4} , since the results are remained almost the same for smaller relative and absolute tolerances.

The first case considered is for an underwater explosion bubble with a maximum equivalent radius $R_{max} = 171.2$ mm initiated at 1.5 m below the water surface, generated by a detonation equivalent to 1.32 g of TNT (Hung & Hwangfu 2010). The computational parameters are chosen as $\kappa = 1.667$, $\varepsilon = 0.0072$, $R_{0*} = 0.1$, $R_{i0*} = 28.1$, and $p_{0*} = 122$ (Wang 2013). Figure 2a shows the history of the local energy of the bubble system versus the history of the bubble radius. The bubble undergoes several cycles of oscillation, each time with reduced amplitude, owing to the loss of the local energy. The local energy remains nearly constant during most of the oscillation, except for very short periods in the vicinity of each minimum volume, when it decreases rapidly. It decreases about 28% during a very short period at the start of the first expansion phase, but remains nearly constant during most of the first cycle of oscillation. The local energy subsequently reduces 47%, 8.5%, 3.9%, 2.3% and 1.4% at the ends of the first to fifth collapse phases, respectively, when a pressure impulse is generated and propagates rapidly through the liquid. It remains as constant at 72%, 25%, 16.5%, 12.6%, 10.3%, and 8.9% of the initial energy during most of the first to sixth cycles of the oscillation. The energy loss due to the acoustic radiation at the minimum volumes of the bubble reduces with oscillation cycles.

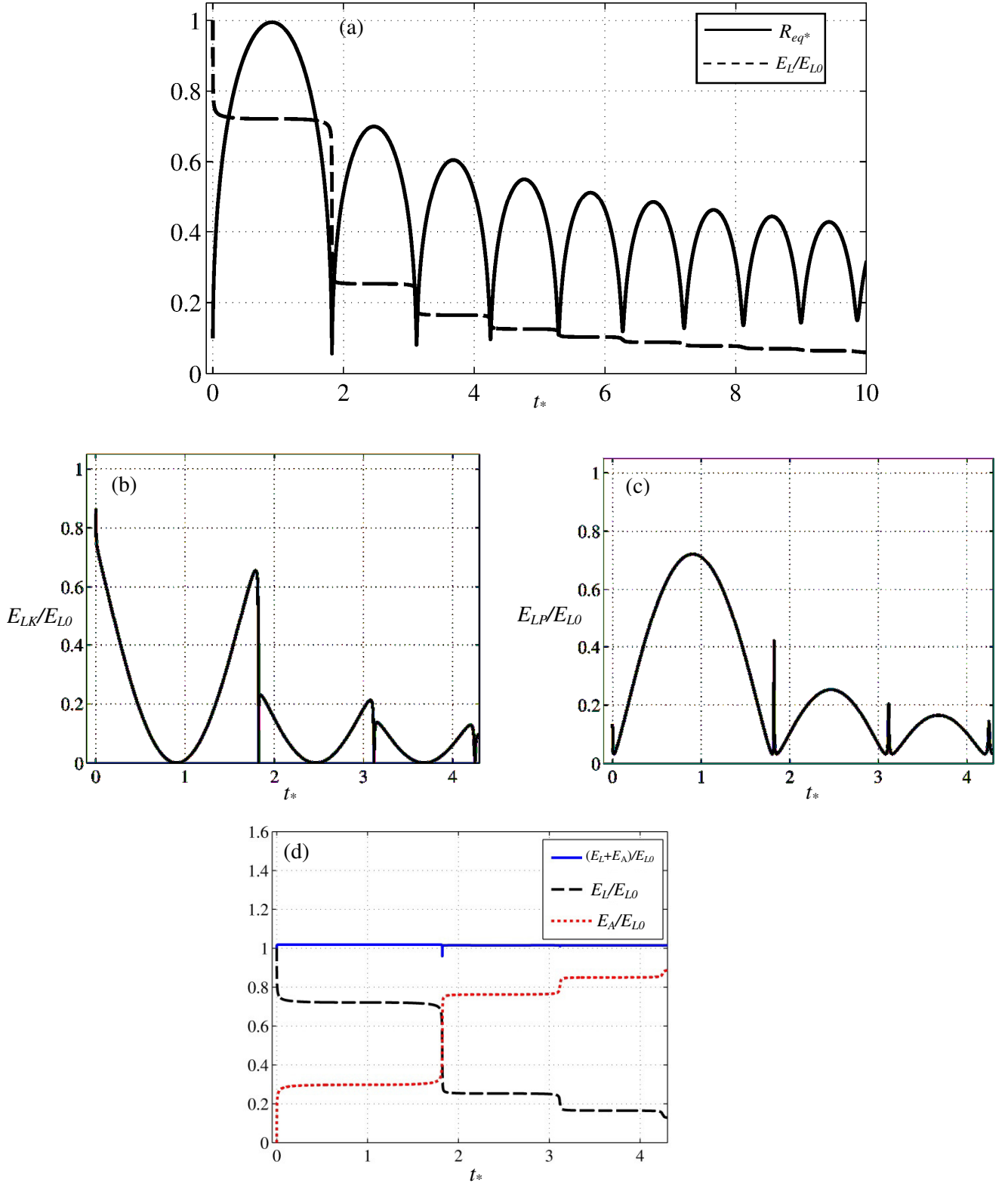


Figure 2. Time histories for the spherical bubble generated by a detonation equivalent to 1.32 g of TNT at 1.5 m below the water surface: (a) the radius R^* and local energy E_L of the bubble system, nondimensionalized by the initial local energy E_{L0} , (b) the local kinetic energy E_{LK} , (c) the local potential energy E_{LP} , and (d) the energy balance. The other parameters used for calculation are $\kappa = 1.667$, $\varepsilon = 0.0072$, $p_{v^*} = 0$, $\sigma^* = 0$, $R_{0^*} = 0.1$, $R_{t0^*} = 28.1$ and $p_{0^*} = 122$.

The time histories of the local kinetic energy and potential energy of the bubble system are shown in figures 2b and 2c, respectively. The local potential energy oscillates in phase with the bubble volume, whereas the local kinetic energy oscillates out of phase with the bubble volume. Their amplitudes decrease significantly from the first to the second cycle and from the second to the third cycle. The spikes at the minimum bubble volumes in figure 2c are due to the contribution from the potential energy of the bubble gases, which achieves maximum values at these moments.

Figure 2d shows the histories of the acoustic radiation energy E_A , the local energy E_L and the total energy E_T . The radiation energy E_A increases for a very short period during each minimum volume of the bubble. The total energy E_T remains approximately constant during all the time considered, which suggests that the main energy loss is due to acoustic radiation and viscous effects are negligible for this case.

Note R_{max} is the maximum bubble radius that a bubble would expand to in an inviscid liquid and without surface tension effects. The difference between unity and the maximum value of R/R_{max} thus reflects the effects of viscosity and surface tension. Figure 3a shows the time history of the bubble radius R/R_{max} for transient bubbles at various initial radii R_0 over a large range from 0.1 μm to 100 mm. The remaining parameters are $\rho_\infty = 1000 \text{ kg m}^{-3}$, $\mu = 0.001 \text{ Pa s}$, $c_\infty = 1500 \text{ m s}^{-1}$, $p_\infty = 100 \text{ kPa}$, $p_v = 0$, $\sigma = 0.07 \text{ N m}^{-1}$, $R_{0*} = 0.1$, $R_{t0*} = 26.7$, $p_{g0*} = 100$, and $\kappa = 1.4$.

As the initial radius R_0 decreases, the damping of the bubble oscillation increases. In the range of R_0 from 0.1 mm to 100 mm, the time history of R/R_{max} does not change with R_0 , where both the viscous effects and surface tension effects are negligible. At $R_0 = 10 \mu\text{m}$, the bubble oscillates only slightly differently from the above results, where viscous and surface tension effects are small. As R_0 is decreased to 1 μm or smaller, the bubble undergoes obviously more severely damped oscillations.

As shown in figure 3b, the local energy E_L follows a step function, falling significantly at the minimum bubble volumes and remaining approximately constant during the remaining time. The energy loss at the minimum bubble volumes decreases with oscillation cycles. In the range of $R_0 = 10 \mu\text{m}$ to 100 mm, the history of E_L does not change significantly with R_0 . The local energy reduces faster for a smaller bubble. At $R_0 = 0.5 \mu\text{m}$, the local energy first falls rapidly due to acoustic radiation and then reduces due to viscous effects. This is repeated during the second cycle. More than two thirds of the local energy is lost for the first cycle of oscillation due to the combined effects of acoustic radiation and viscosity.

Figure 3c shows the time history of the total energy E_T . In the range of $R_0 = 0.1 \text{ mm}$ to 100 mm, the total energy remains almost constant, with viscous effects being negligible. It only reduces about 0.4% at the end of the first collapse phase, which should be due to the approximation of the Keller–

Miksis equation. Note that the Keller–Miksis equation is based on a weakly compressible theory to second order.

For $R_0 = 10, 5 \mu\text{m}$, the total energy E_T remains about 97% and 93.5% (figure 3c), respectively, in the fifth oscillation, and therefore the corresponding energy loss due to viscous effects are 3% and 6.5%, respectively. At the same time, the local energy remains 19% and 18% of the initial value (figure 3b), respectively, and the energy loss due to compressible effects are thus 78% and 75.5%, respectively. This suggests that the loss of the local energy is mainly due to acoustic radiation and viscous effects are negligible when R_0 is equal to $5 \mu\text{m}$ or larger.

Both compressible effects and viscous effects are essential for microbubble dynamics. For $R_0 = 1 \mu\text{m}$, the energy loss due to viscous effects is 18% and 28% after the first and fourth cycles of oscillation, respectively, when the corresponding energy loss due to acoustic radiation is 54% and 60%, respectively. The local energy is lost faster for a smaller bubble. For $R_0 = 0.5 \mu\text{m}$, the loss of the local energy after the first oscillation is about 76%, of which 44% is due to compressible effects and 32% due to viscous effects. The energy loss after the first four cycles of oscillation is about 90%, of which 48% is due to compressible effects and 42% due to viscous effects. For $R_0 = 0.1 \mu\text{m}$, the energy of the bubble system is lost mostly during the first oscillation. The loss of the local energy during the early expansion is about 58%, of which 36% is due to compressible effects and 22% due to viscous effects. The energy loss after the first cycle of oscillation is about 85%, of which 24% is due to compressible effects and 61% due to viscous effects.

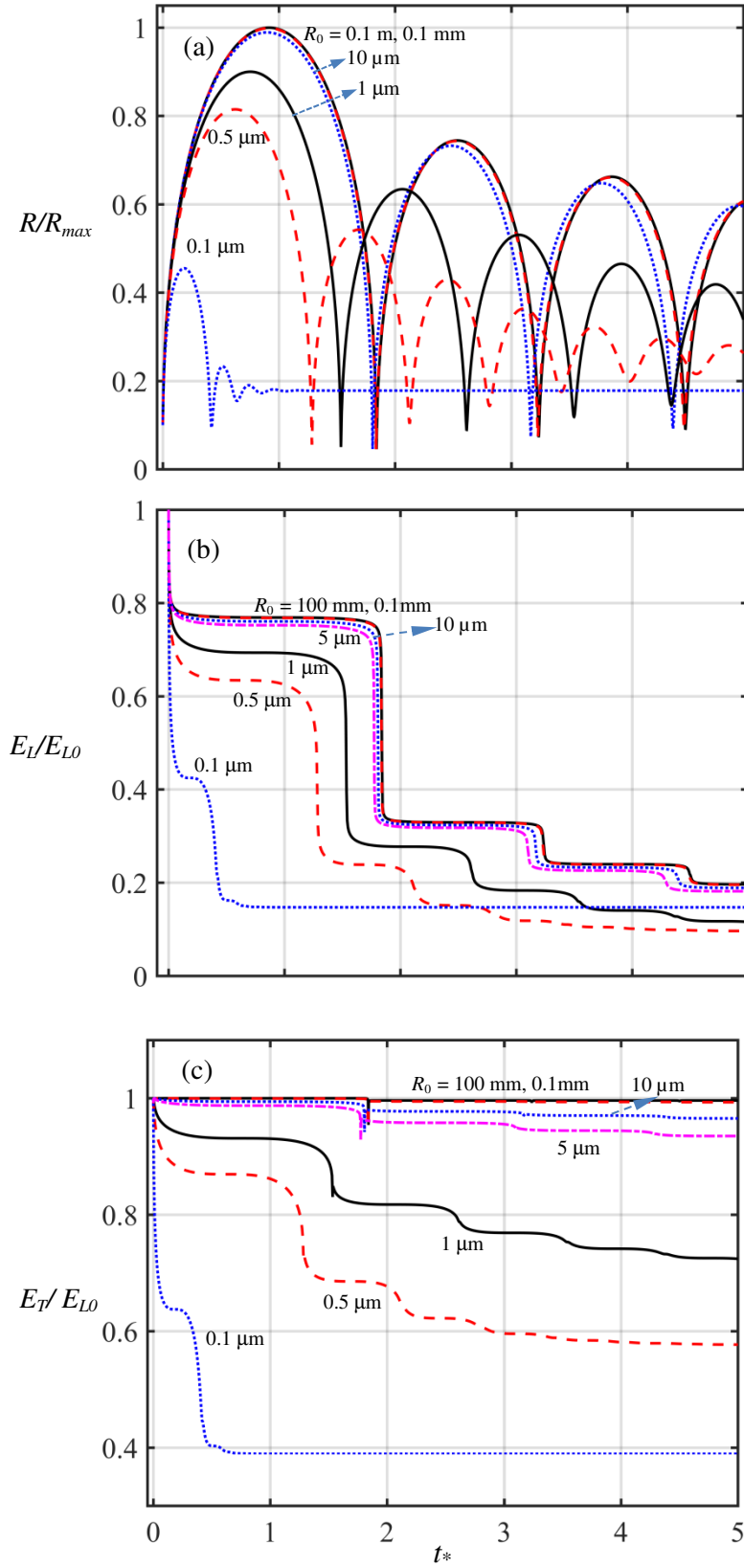


Figure 3. Time histories of (a) the dimensionless bubble radius R/R_{max} , (b) local energy of the bubble system E_L/E_{L0} , and (c) total energy E_T/E_{L0} , for transient bubbles with initial radius R_0 ranging from $0.1 \mu\text{m}$ to 100 mm . The other parameters are $\rho_\infty = 1000 \text{ kg m}^{-3}$, $\mu = 0.001 \text{ Pa s}$, $c_\infty = 1500 \text{ m s}^{-1}$, $p_\infty = 100 \text{ kPa}$, $p_v = 0$, $\sigma = 0.07 \text{ N m}^{-1}$, $R_{0*} = 0.1$, $R_{t0*} = 26.7$, $p_{g0*} = 100$, and $\kappa = 1.4$.

Figure 4 shows the time histories of the dimensionless bubble radius R_* , and local energy E_L/E_{L0} , for transient bubbles for $\sigma_* = 0.07$ and $Re = 10, 100, 300$ and 1000 , respectively. Other parameters used are $\varepsilon = 0.00667$, $p_{v*} = 0$, $R_{0*} = 0.1$, $R_{t0*} = 26.7$, $p_{g0*} = 100$, and $\kappa = 1.4$. With the decrease of the Re number, both the oscillation period and maximum bubble radius decrease, whereas the minimum radius increases. For $Re = 1000$, the total energy loss is 84% after the first four cycles of oscillation, of which 80% is due to compressible effects and 4% due to viscous effects. For $Re = 300$, the total energy loss is 72% after the first oscillation, of which 66% is due to compressible effects and 6% due to viscous effects. The total energy loss is 85% after the first four cycles of oscillation, of which 74% is due to compressible effects and 11% due to viscous effects. Compressible effects are thus dominant for $Re = 300$ or larger.

Both compressible effects and viscous effects are essential for $Re = 100$ or smaller. For $Re = 100$, the total energy loss is 89% after the first four cycles of oscillation, of which 61% is due to compressible effects and 28% due to viscous effects. For $Re = 10$, the total energy loss is 92% after the first four cycles of oscillation, of which 34% is due to compressible effects and 68% due to viscous effects.

Note here that the Reynolds number Re is defined in terms of the maximum bubble radius R_{max} . The Reynolds number is also often defined in terms of the initial bubble radius, $Re_0 = \rho UR_0/\mu$. As $R_0 = 0.1R_{max}$ in the cases, $Re_0 = 0.1Re$.

Figure 5 shows the effects of surface tension. The oscillation period and maximum bubble radius decrease with the dimensionless surface tension σ_* , but the loss of the local energy does not change significantly with σ_* .

Figure 6 shows the comparison between the Keller–Miksis equation (KM) and the compressible BIM model, for the time histories of the dimensionless bubble radius R_* and the local energy E_L/E_{L0} , for a transient bubble for $R_0 = 100 \mu\text{m}$. The BIM results are calculated for the number of nodes $n = 41, 51$, respectively, showing convergence of the numerical model in terms of the mesh size. The BIM results agree very well with that of the Keller–Miksis equation. This is as expected, since both the Keller–Miksis equation and the compressible BIM model are based on the weakly compressible theory to second order in terms of the Mach number ε . Lezzi & Prosperetti (1987) compared the third order solution with the second order solution. They noticed that the second order theory describes the main compressible effects when the Mach number is small, and the third order solution is a minor correction.

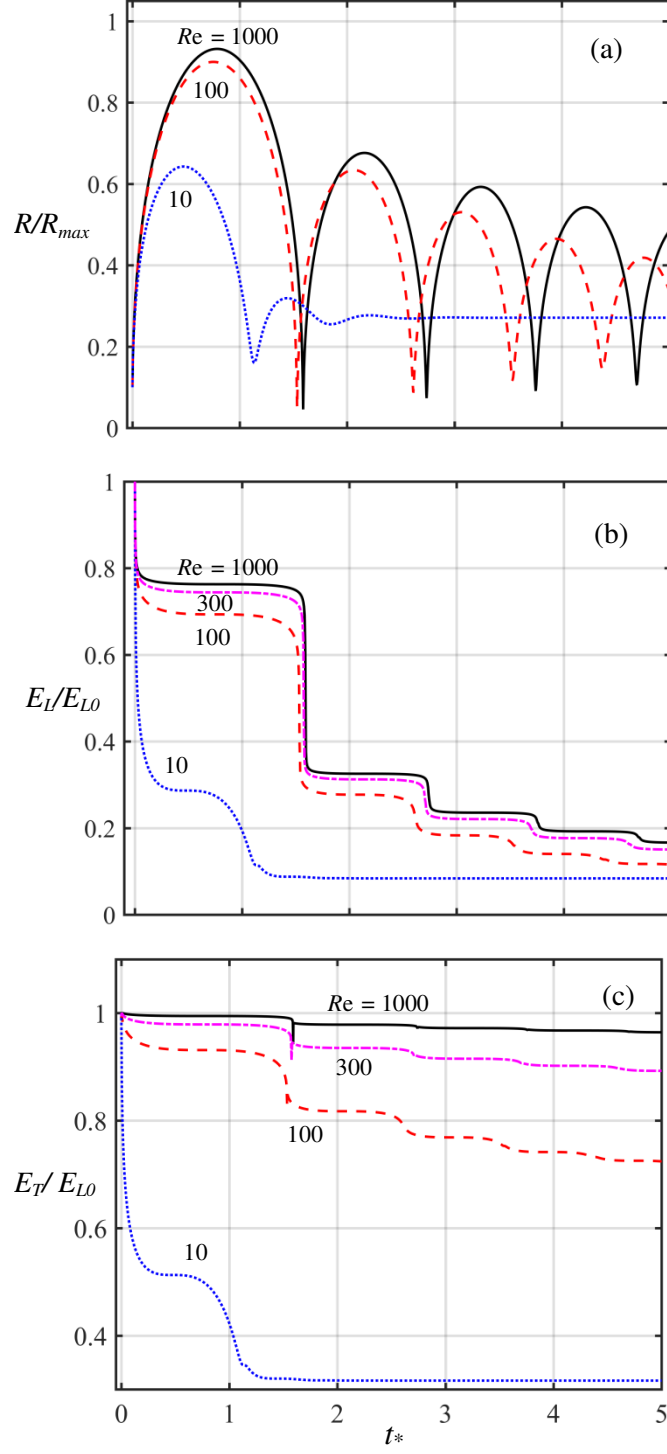


Figure 4. Time histories of (a) the dimensionless bubble radius R/R_{max} , (b) local energy E_L/E_{L0} , and (c) the total energy $E_T/\max(E_T)$, for transient bubbles for $\sigma^* = 0.07$ and $Re = 10, 100, 300, 1000$, respectively. Other parameters are $\varepsilon = 0.00667$, $p_v^* = 0$, $R_0^* = 0.1$, $R_{t0}^* = 26.7$, $p_{g0}^* = 100$, and $\kappa = 1.4$.

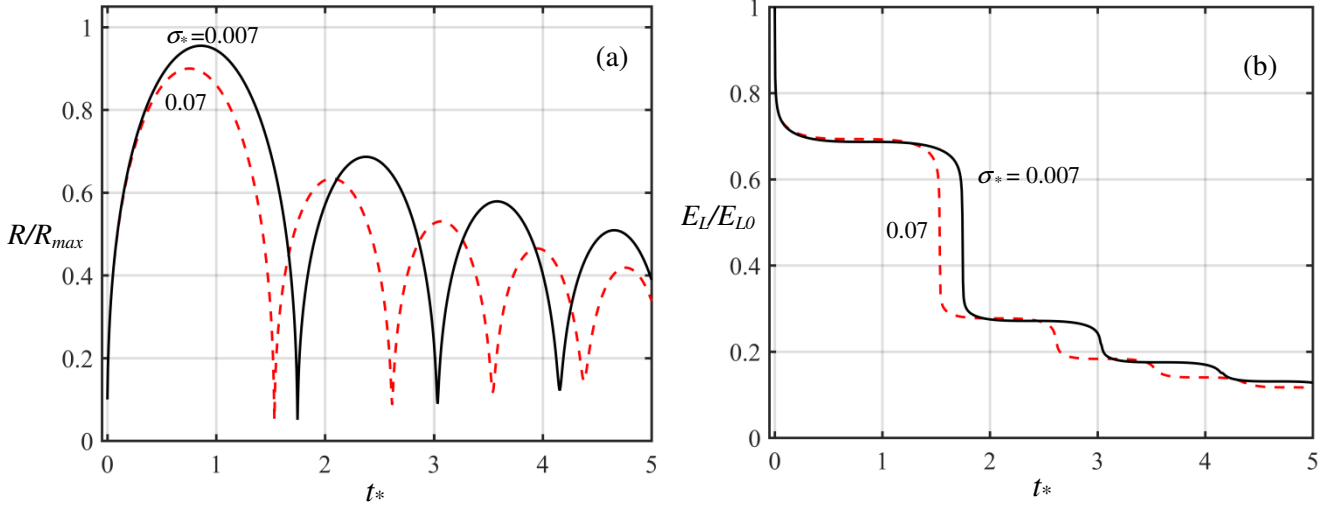


Figure 5. Time histories of (a) the dimensionless bubble radius R/R_{max} , and (b) local energy E_L/E_{L0} , for transient bubbles for $Re = 100$ and $\sigma_* = 0.007, 0.07$ respectively. Other parameters are the same as figure 4.

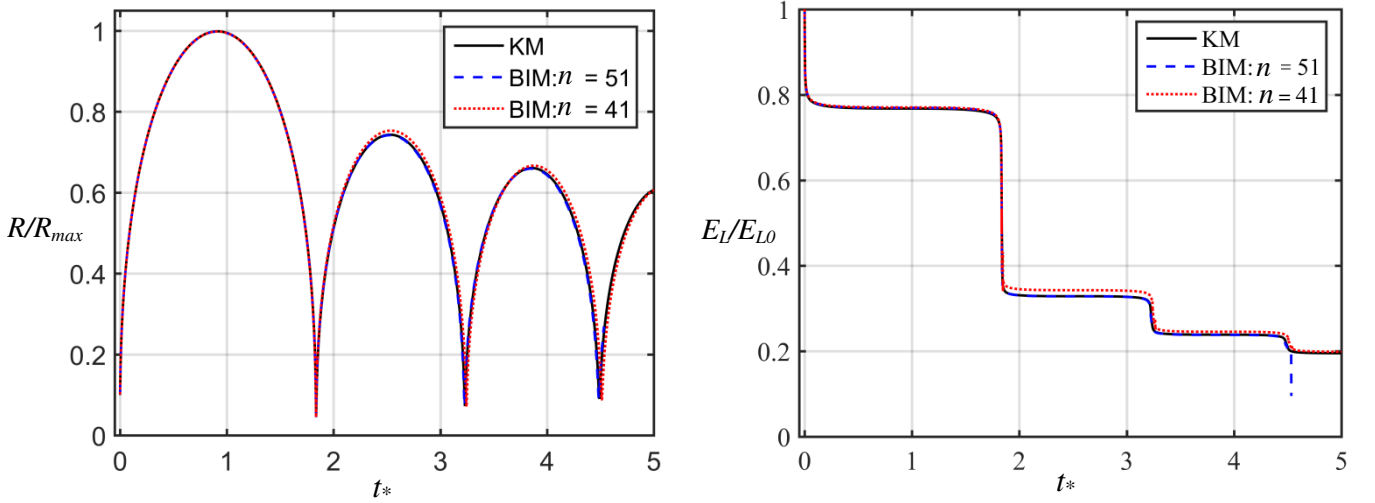


Figure 6. Comparison between the Keller–Miksis equation (KM) and BIM modelling for the number of nodes $n = 41, 51$, respectively, for the time histories of (a) the dimensionless bubble radius R/R_{max} , and (b) local energy E_L/E_{L0} , for a transient bubble for $R_0 = 100 \mu\text{m}$. Other parameters are the same as figure 3.

5. A gas bubble under buoyancy

We now consider a nonspherical bubble generated by an underwater explosion at $R_m = 171$ mm and depth $h = 1.5$ m from the water surface. The bubble shapes calculated for this case using the recently developed compressible BIM model (Wang 2013) agree well with experiments (Hung & Hwangfu 2010) for both the first and second cycles of oscillation (see figure 7). The bubble expands spherically, reaching the first maximum volume (sequence 1), and then collapses spherically. However the lower part of the bubble surface is flattened due to buoyancy at the end of collapse (sequence 2), whereupon an upward jet forms, impacts the opposite bubble surface and subsequently penetrates the bubble. The bubble re-expands to a spherical shape at its second maximum volume (sequence 3) and then re-collapses with a jet forming at the end of re-collapse (sequence 4). It further rebounds with a sharp jet (sequence 5).

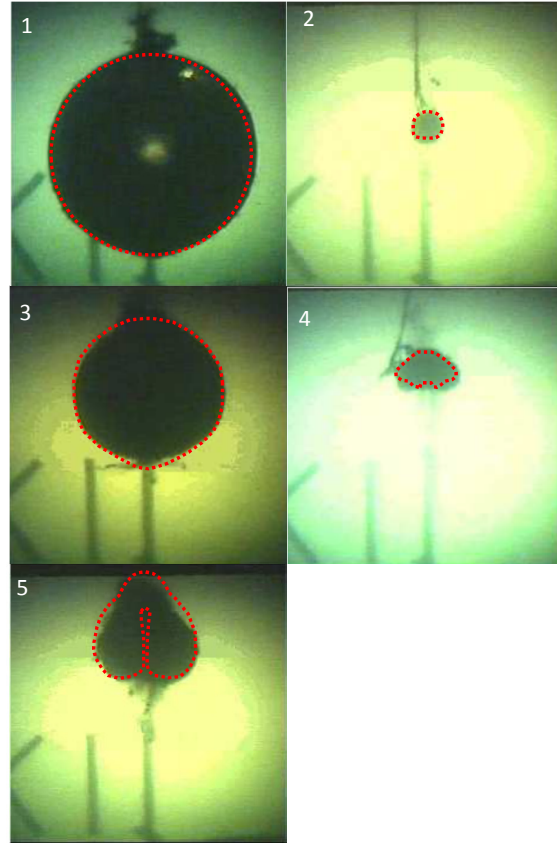


Figure 7. Comparison of the compressible BIM model computation (dotted line) with the experimental images (Hung & Hwangfu 2010) for an underwater explosion bubble at $R_m = 171$ cm and the depth $h = 1.5$ m below the water surface, at times $t = 15, 27, 36, 48, 51$ ms. The image width is 500 mm. Other parameters are $\kappa = 1.667$, $R_0/R_m = 0.1$, $R_{t0} = 303 \text{ m s}^{-1}$, $p_{\infty} = 116 \text{ kPa}$ and $p_0 = 14.2 \text{ MPa}$.

Figure 8a shows the time history of the local energy E_L of the bubble system versus the equivalent bubble radius $R_{eq*} = \left(\frac{3}{4\pi}V_*\right)^{1/3}$. A substantial part, 26.5%, of the local energy is lost during a very short period at the inception of the bubble, when a steep pressure wave is emitted with high pressure amplitude. It remains almost constant at 73.5% of the initial energy for most of the time during the first cycle but decreases rapidly and significantly at the end of collapse, with the emission of another steep pressure wave. About 35% of the initial energy is lost this time with only about 38.5% of the initial energy left during the second cycle. As a result, the dimensionless maximum radius reduces from 1.0 during the first cycle to 0.79 during the second cycle. About 27% of the initial energy is lost around the end of recollapse with only 11.5% of the initial energy left during the third cycle of oscillation. The dimensionless maximum radius reduces further to 0.53 during the third cycle. The local energy of the bubble system is conserved during most of the time, except for very short periods around the minimum volumes of the bubble.

Figure 8b shows that the local potential energy E_{LP} of the bubble system oscillates in phase with the bubble volume while the local kinetic energy E_{LK} oscillates out of phase with the bubble volume. Both of their magnitudes reduce significantly from the first to the second cycles of oscillation and from the second to the third cycles.

Figure 9 shows that the local energy appears as a step function of time for underwater explosion bubbles for various buoyancy parameters $\delta = 0.12, 0.2$ and 0.3 , corresponding to $R_m = 171, 476$, and 1000 mm, respectively. With the initial energy deposited from the explosion, the bubble expands rapidly at inception with the emission of a steep pressure wave; the local energies then fall by about 27% for all three bubbles, when they are small and the buoyancy effects are negligible. The local energy is conserved while the bubbles oscillate but falls rapidly at the end of collapse, when another steep pressure wave is emitted. A larger bubble is associated with stronger buoyancy effects and a stronger liquid jet formed at the end of collapse (Wang 2013), and thus its collapse is weaker with less energy loss. Consequently, the energy of the bubble system remains at about 39%, 45% and 54% of the initial energy during the second cycle of oscillation for $R_m = 171, 476$, and 1000 mm, respectively.

This model does not simulate the propagation of pressure waves, but it models the rapid and significant losses of the local energy at the inception of a bubble and the end of collapse. This rapid and significant energy loss should be associated with a steep pressure wave in a narrow region travelling through water. After it propagates radially for a while its amplitude will drop, because the surface wave front is approximately spherical with its area increasing with time.

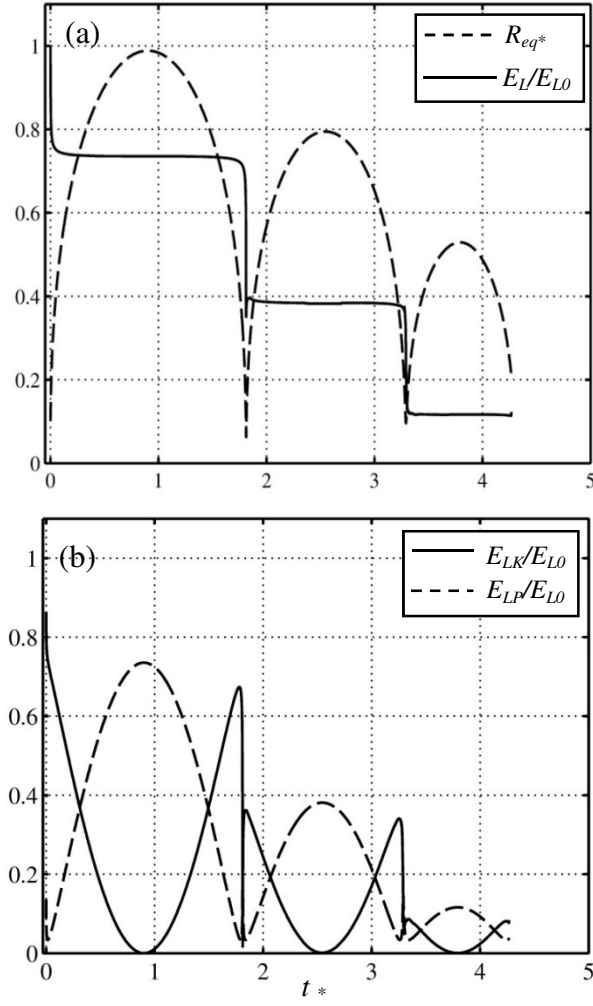


Figure 8. Time histories of the bubble system for the case shown in figure 7: (a) the equivalent bubble radius R_{eq}^* and the local energy E_L of the bubble system and (b) the local kinetic energy E_{LK} and potential energy E_{LP} . The energy is nondimensionalized by the initial local energy E_{L0} .

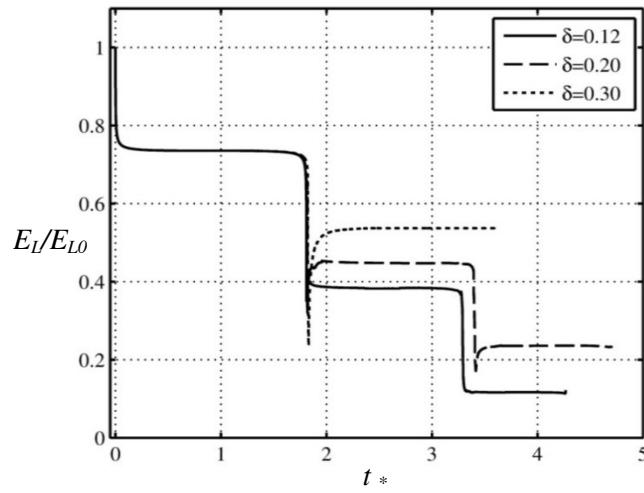


Figure 9. Time histories of the local energy E_L of the bubble system for various buoyancy parameters $\delta = 0.12, 0.2$ and 0.3 , with the remaining parameters being the same figure 7.

One of the damage mechanisms of underwater explosions is associated with the steep pressure wave emitted at inception of the underwater explosion bubble (Wardlaw et al. 2000, 2003a, b). Another damage mechanism is associated with the high-speed liquid jet formed at the end of collapse (Chahine et al. 1988, 1998a, b, Duncan et al. 1993, 1996, Blake et al. 1997, Wang 1998, 2004), which is often directed towards a nearby structure (Chahine et al. 1980, Klaseboer et al. 2005, Jayaprakash et al. 2010, 2011).

6. A cavitation bubble near a rigid wall

This section is concerned with cavitation bubble dynamics near a rigid boundary. The cases considered are for a bubble with $R_m = 1.45$ mm at various standoff distance from the boundary, which correspond to the experimental cases by Philipp & Lauterborn (1998). The other computational parameters chosen are $\kappa = 1.4$, $\varepsilon = 0.013$, $\sigma^* = 0.00051$, $R_{0*} = 0.1$, $R_{l0*} = 31$ and $p_{g0*} = 127$. The bubble shapes calculated for these cases, using the compressible BIM model (Wang 2014) agree well with the experiment for both the first and second cycles of oscillation.

The first case is for a bubble at the dimensionless standoff distance $\gamma = s/R_m = 3.0$ from the rigid boundary, where s is the distance of the bubble centre from the rigid boundary at inception. Figure 10a shows the time history of the local energy E_L of the bubble system versus the time history of the bubble equivalent radius R_{eq*} for the first and second cycles of oscillation. The local energy remains constant except for very short periods around the minimum bubble volumes, where it reduces rapidly. The local energy falls about 44% during its inception and remains at 56% of the initial energy during most of the first cycle of oscillation. It further reduces by 32% during the end of collapse and remains at 24% of the initial energy during the second cycle.

Figure 10b shows that the local potential energy E_{LP} of the bubble system oscillates in phase with the bubble volume while the local kinetic energy E_{LK} is out of phase with the bubble volume. Both of their magnitudes reduce significantly from the first to the second cycles of oscillation.

Figure 10c shows the time histories of the local energy E_L of the bubble system at various dimensionless standoff distances from the rigid boundary for $\gamma = 3.0$, 2.0 and 1.6, respectively. At inception it falls by about 44% at all three standoff distances, when the bubble is small and the effects of the boundary are negligible. The bubble becomes nonspherical during the later stage of collapse, when a high-speed liquid jet forms towards the boundary. When the bubble is nearer to the boundary a stronger jet forms and the collapse becomes relatively weaker (Philipp & Lauterborn 1998, Wang 2014). As a result, the energy loss decreases as the bubble is initiated nearer the boundary, remaining at about 24%, 36% and 45% of the initial energy in the second cycle of oscillation for $\gamma = 3.0$, 2.0 and 1.6, respectively. The local energy loss at the end of collapse decreases rapidly, as the standoff distance is decreased. This is true because when the bubble is

closer to the boundary, the bubble becomes nonspherical earlier in its oscillation cycle, a larger jet then forms and a larger amount of kinetic energy is associated with the jet (Zhang et al. 1993, 1994, Philipp & Lauterborn 1998, Wang 2014). Consequently, the bubble collapse becomes relatively weaker.

Cavitation damage is generally believed to be due to shock wave emission and bubble jetting formed at the end of collapse (Rayleigh 1917, Taylor 1942, Naud'e & Ellis 1961, Plesset & Chapman 1971, Plesset & Prosperetti 1977, Blake & Gibson 1987). It was suggested by experimental studies (Tomita & Shima 1986, Philipp & Lauterborn 1998, Wang, Liu, et al. 2015) that cavitation erosion is also associated with a bubble ring with high pressure and temperature in direct contact with a rigid boundary formed at the end of recollapse. Chen & Israelachvili (1991) noticed in experiments that the inception of cavities is intimately connected with simultaneous relaxations of high local strain energies on nearby surfaces. They suggest that in many practical situations, damage is more likely to occur during the formation, rather than the collapse, of cavities. The damage mechanism of Chen & Israelachvili (1991) is consistent with the result observed here that the local energy of a bubble system at inception is much higher than at the end of collapse.

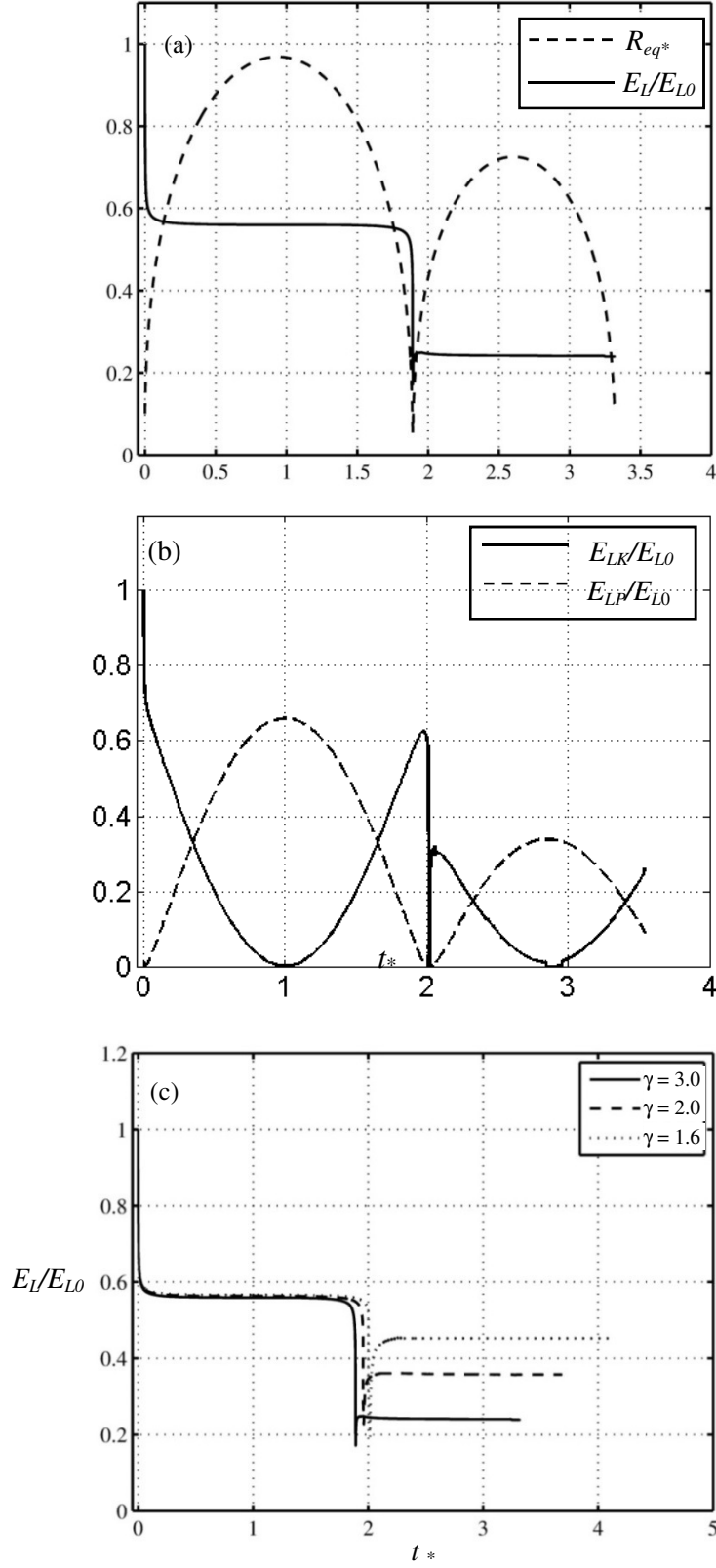


Figure 10. Time histories of cavitation bubble dynamics near a rigid boundary characterized by $\kappa = 1.4$, $\varepsilon = 0.013$, $\sigma^* = 0.00051$, $R_{0^*} = 0.1$, $R_{i0^*} = 31.0$, $p_{v^*} = 0$ and $p_{g0^*} = 127$: (a) the equivalent bubble radius R_{eq}^* and the local energy E_L of the bubble system for $\gamma = 3.0$, (b) the local kinetic energy E_{LK} and potential energy E_{LP} for $\gamma = 3.0$, and (c) the comparison of the local energy at various standoff distances from the rigid boundary for $\gamma = 3.0$, 2.0 and 1.6, respectively.

7. Single bubble sonoluminescence

Single bubble sonoluminescence is an intriguing phenomenon. A gas bubble of only a few micrometres in size is levitated in a liquid by an acoustic standing wave and kept in position at a pressure antinode. As the bubble is compressed periodically by the acoustic wave, it emits light pulses so intense as to be visible to the naked eye with clock-like regularity (Suslick & Crum 1997, Gaitan et al. 1992, Gompf et al. 1997, Hiller et al. 1992, Lohse 2005). This process gives rise to featureless continuum emission in water (from 200 to 800 nm, with increasing intensity into the ultraviolet) (Hiller et al. 1992, 1998).

The initial pressure of a gas bubble at equilibrium is given as, $p_{g0} = p_{\infty} + 2\sigma/R_0$, which is in balance with the ambient pressure and surface tension. The pressure at the antinode of a standing wave is

$$p_a(t) = -p_A \sin(2\pi ft), \quad (7.1)$$

where p_A and f are the amplitude and frequency of the acoustic wave, respectively.

A typical sonoluminescence case is considered using the Keller–Miksis equation, with the parameters chosen as $p_A = 130$ kPa, $f = 20$ kHz and $R_0 = 5$ μm (Lauterborn & Kurz 2010). As shown in figure 11a, the local energy first increases rapidly from nearly zero to its maximum value, within a very short period (about 10 μs , 20% of the wave period), by absorbing energy from the acoustic wave. The local energy then decreases more rapidly to nearly zero in about 4 μs (8% of the wave period) and remains small during the remainder of the cycle, for about 35 μs (70% of the wave period). The majority of the energy loss (about 80%) happens within 0.1 μs , which is only 0.2% of the wave period. As a result, the gas bubble in water is driven into violent oscillation. It expands to more than eight times its ambient radius, and then collapses rapidly over a very short time period (about 4 μs). The bubble subsequently vibrates with small amplitude at approximately its natural frequency.

As shown in figures 11b and 11c, the potential energy of the bubble gas is small most of the time except for a very short period near the minimum bubble volumes. The gas potential energy is appreciable within a time span of 0.01 μs (0.02% of the wave period) at the end of the violent collapse, achieving its maximum of $0.18 \max(E_L)$, when the bubble is small at $R = 0.675$ μm and the energy density of the bubble gas is large at 3.5×10^{25} J M^{-3} . In reality, the energy density cannot reach this value due to the evaporation of water, heat transfer and emission of light (Szeri et al. 2003, Lohse 2005, Zhang & Li 2014). This energy concentration yields very high pressures and temperatures, thus providing the physical internal environment for sonoluminescence and sonochemistry. The local energy describes the energy transfer from the acoustic wave to the bubble system and the subsequent energy concentration due to the bubble collapse.

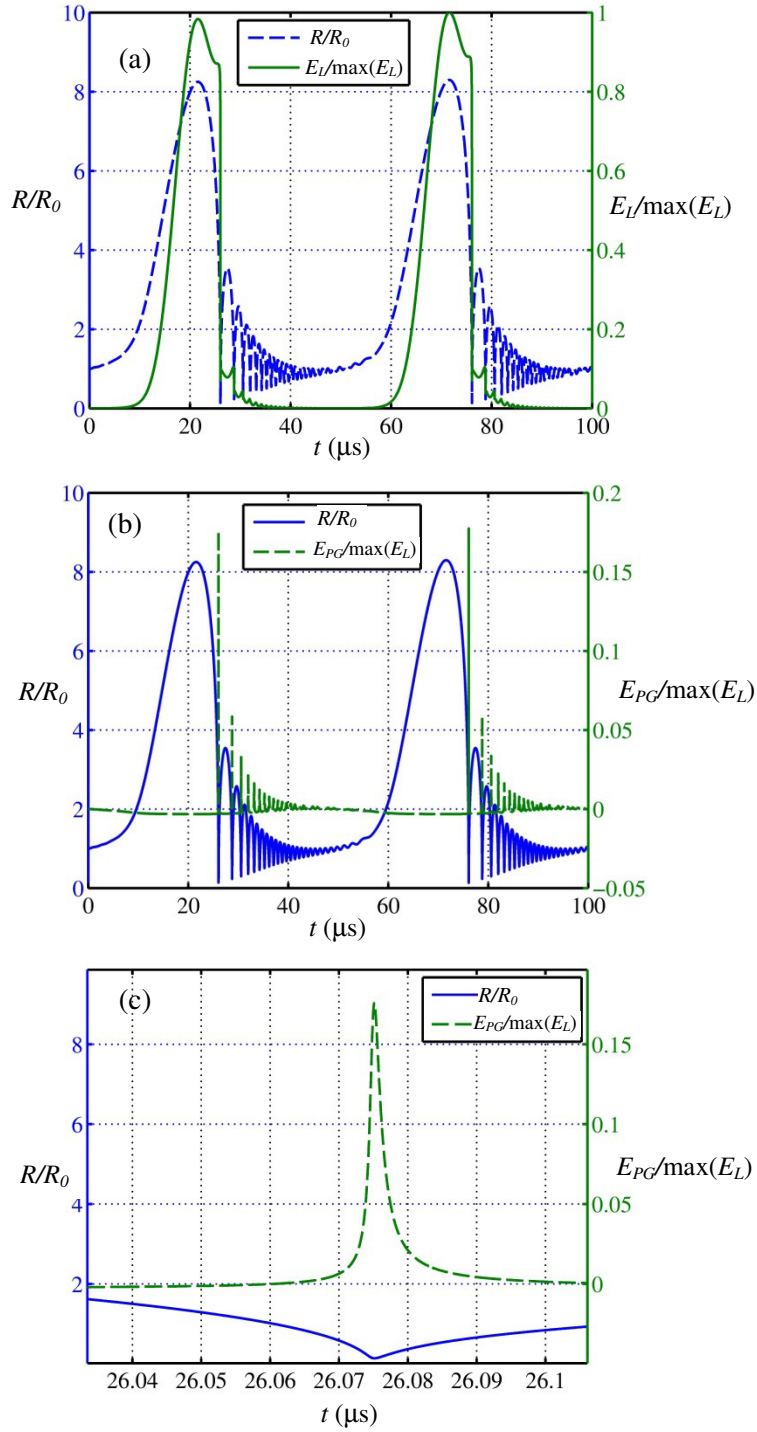


Figure 11. Time histories of a bubble with an initial radius $R_0 = 5 \mu\text{m}$ and initial pressure $p_{g0} = 1.3$ atm (0.3 atm due to surface tension) at the anti-node of a standing wave having pressure amplitude $p_A = 1.3$ atm and frequency $f = 20$ kHz: (a) the local energy E_L of the bubble system and the bubble radius R versus time, (b) the potential energy E_{PG} of the bubble gas and the bubble radius R versus time, and (c) an enlarged view of the gas potential energy E_{PG} and radius R near the end of the first collapse.

8. Summary and conclusions

The total mechanical energy E_T of a bubble system consists of the local energy E_L within the inner asymptotic region and the acoustic radiation energy E_A radiated to the far field, i.e.

$$E_T = E_L + E_A. \quad (8.1)$$

The local energy of a bubble system E_L consists of the local potential energy E_{LP} of the bubble system and the local kinetic energy E_{KL} of the liquid flow in the inner region,

$$E_L = E_{PL} + E_{LK} = \frac{p_{g0} V_0}{\kappa - 1} \left(\frac{V_0}{V} \right)^{\kappa - 1} + \sigma A - \rho_\infty g V z_c + (p_\infty - p_v) V + \frac{1}{2} \rho_\infty \oint_S \phi \phi_n dS + O(\varepsilon), \quad (8.2)$$

where p_{g0} is the initial pressure of the bubble gas, V_0 and V are the initial and transient bubble volumes, respectively, κ is the polytropic index of the bubble gas, p_v is the partial pressure of vapour inside the bubble, σ is surface tension, A is the area of the bubble surface, g is the acceleration of gravity, z_c is the z -coordinate (opposite to the direction of gravity) of the geometric centre of the bubble, ρ_∞ and p_∞ are the density and pressure of the undisturbed liquid, respectively, ϕ and ϕ_n are the potential and normal velocity on the bubble surface, respectively, and $\varepsilon = \sqrt{(p_\infty - p_c) / \rho_\infty} / c_\infty$ is the bubble wall Mach number, where c_∞ is the speed of sound in the undisturbed liquid. The order of the errors in (8.2) should be for the corresponding dimensionless equation.

The energy radiated outside of the inner region due to acoustic radiation from the start to the present time t is given by

$$E_A(t) = C_0 \frac{\rho_\infty}{c_\infty} \left\{ \dot{V}(0) \ddot{V}(0) - \dot{V}(t) \ddot{V}(t) + \int_0^t \ddot{V}^2(t) dt \right\} + O(\varepsilon^2), \quad (8.3)$$

where C_0 is $1/(4\pi)$ or $1/(2\pi)$ for a bubble in an unbounded liquid or near a rigid flat boundary, respectively, and the overdots denote the derivative with respect to time t . The local energy loss due to radiation depends on the history of the bubble volume alone to first order. The transient energy flux N_{flux} to the far field is given as

$$N_{flux} = -C_0 \frac{\rho_\infty}{c_\infty} \dot{V}(t) \ddot{V}(t) + O(\varepsilon^2). \quad (8.4)$$

As the energy is lost irreversibly through acoustic radiation, the bubble system with the remaining local energy undergoes damped oscillation, with both the amplitude and period decreasing significantly with time. Thus, it is the local energy at the time considered not the total energy that determines the bubble motion and the associated forces, stresses, momentum and mass and heat transfer.

We have analysed the time histories of the local energy for the oscillation of spherical bubbles, underwater explosion bubbles with buoyancy effects, laser-generated bubbles near a rigid boundary, as well as spherical bubbles oscillating stably in a standing acoustic wave. Various mechanisms and

properties of the energy associated with bubble dynamics have been identified in this study, which are summarized as follows.

If the Reynolds number in terms of the initial bubble radius is 30 or larger, the loss of the local energy for the cases considered is primarily associated with acoustic radiation. For cases with smaller Reynolds numbers, both compressible and viscous effects contribute to the local energy loss.

The local energy is lost rapidly and substantially at bubble inception due to emission of a shock wave. The local energy then remains almost constant for most of the first cycle of oscillation, when viscous effects are small. This process is repeated, except the energy loss at the minimum bubble volume decreases with subsequent oscillation cycles.

The local potential energy of a bubble system oscillates in phase with the bubble volume while the local kinetic energy oscillates out of phase with the bubble volume. Both of their magnitudes decrease significantly with oscillation cycles. The potential energy of the bubble gases increases inversely with the bubble volume.

The loss of the local energy of a bubble system and the associated damping of the bubble oscillation are diminished by buoyancy effects and reduce with the buoyancy parameter. This is true because a substantial portion of the kinetic energy is associated with the liquid jet generated by buoyancy. Consequently, the bubble collapse becomes weaker and less energy is radiated through the acoustic wave to the far field. Similarly, the loss of the local energy of a bubble system and the associated damping of the bubble oscillation are diminished by the presence of a rigid boundary and decrease with proximity of the bubble to the boundary.

A microbubble driven at the antinode of a standing wave has quite different properties from those discussed above. This bubble absorbs substantial energy from the acoustic wave and oscillates violently yet stably. The local energy of the bubble system increases rapidly from nearly zero to its maximum within a very short time period and then decreases more rapidly to nearly zero, having a small value during the rest of the oscillation. The majority of the energy loss happens rapidly during about 0.2% of the wave period for the case considered here. The potential energy of the bubble gas is at an extremely high density at the end of the violent collapse for about 0.02% of the wave period, yielding very high pressures and temperatures, and thus providing the physical internal environment for sonoluminescence and sonochemistry. The local energy describes the energy transfer from the acoustic wave to the bubble system and the subsequent energy concentration due to the bubble collapse.

ACKNOWLEDGMENTS

The author would like to express his sincere thanks to Professor John R. Blake and Dr. Michael Calvisi for their valuable comments on the manuscript as well as the associate editor for his valuable comments and suggestions during the review process.

References

- Akhatov, I., Lindau, O., Topolnikov, A., Mettin, R., Vakhitova, N. and Lauterborn, W. 2001 Collapse and rebound of a laser-induced cavitation bubble. *Phys. Fluids* **13**, 2805.
- Benjamin, T. B. and Ellis, A. T. 1966 The collapse of cavitation bubbles and the pressure thereby produced against solid boundaries. *Phil. Trans. R. Soc. Lond. A* **260** 221–40
- Best, J. P. 1993 The formation of toroidal bubbles upon collapse of transient cavities. *J. Fluid Mech.* **251**, 79-107.
- Blake, J. R. 1988 The Kelvin impulse: Application to cavitation bubble dynamics. *J. Austral. Math. Soc. B30*, 127–146.
- Blake, J. R. and Gibson, D. C. 1987 Cavitation bubbles near boundaries. *Annu. Rev. Fluid Mech.* **19**, 99-123.
- Blake, J. R., Hooton, M. C., Robinson, P. B. and Tong, P. R. 1997 Collapsing cavities, toroidal bubbles and jet impact. *Phil. Trans. R. Soc. Lond. A* **355**, 537-550.
- Brennen, C. E. 1995 *Cavitation and Bubble Dynamics*, Oxford University Press (available online).
- Brujan, E. A. and Matsumoto, Y. 2012 Collapse of micrometer-sized cavitation bubbles near a rigid boundary. *Microfluid Nanofluid.* **13**, 957–966.
- Calvisi, M. L., Ilroeta, J. I. and Szeri, A. J. 2008 Dynamics of bubbles near a rigid surface subjected to a lithotripter shock wave: II. Reflected shock intensifies nonspherical cavitation collapse *J. Fluid Mech.* **616** 63–97
- Chahine, G.L. and Bovis, A. 1980 Oscillation and collapse of a cavitation bubble in the vicinity of a two-liquid interface. *Cavitation and Inhomogeneities in Underwater Acoustics*, Springer-Verlag ed. New York, pp. 23-29.
- Chahine G.L. and Harris G. 1998a Multi-Cycle underwater explosion bubble model. Part I: Theory and validation examples for free-field bubble problems. U.S. Naval Surface Warfare Center Indian Head Division, Report IHCR 98-64, June 1998.
- Chahine, G.L. and Harris, G. 1998b Multi-Cycle underwater explosion model. Part II: Validation Examples for Hull Girder Whipping Problems. U.S. Naval Surface Warfare Center Indian Head Division, Report IHCR 98-65, June 1998.
- Chahine, G.L. and Hsiao, C-T. 2015 Modelling Cavitation Erosion using Fluid – Material Interaction Simulation. *Interface Focus*, **5**, 20150016. <http://dx.doi.org/10.1098/rsfs.2015.0016>.
- Chahine, G.L., Kapahi, A., Choi, J.-K., and Hsiao, C.-T. 2016 Modeling of surface cleaning by cavitation bubble dynamics and collapse. *Ultrasonics Sonochemistry*, **29**, 528-49.
- Chahine, G. L. and Perdue, T. O. 1988 Simulation of the three-dimensional behaviour of an unsteady large bubble near a structure. In *Proc. 3rd Intl Colloq. on Drops and Bubbles*, Monterey, CA.
- Chen, Y.L., Israelachvili, J. 1991 New mechanism of cavitation damage. *Science*, **252**, 1157 - 1160.
- Cole, R. H. 1948 *Underwater Explosions*. Princeton University Press.
- Coussios, C. C. and Roy, R. A. 2007 Applications of Acoustics and Cavitation to Non-invasive Therapy and Drug Delivery. *Annu. Rev. Fluid Mech.* **40**, 395-420.
- Curtiss, G. A., Leppinen, D. M., Wang, Q. X. and Blake, J. R. 2013 Ultrasonic cavitation near a tissue layer. *J. Fluid Mech.* **730**, 245-272.
- Delius, M. 1990 Effect of lithotripter shock waves on tissues and materials. In *Proc. 12th ISNA: Frontiers of Nonlinear Acoustics* (ed. M. F. Hamilton and D. T. Blackstock), 31-46. Elsevier.
- Duncan, J. H., Milligan, C. D. and Zhang, S. G. 1996 On the interaction between a bubble and a submerged compliant structure. *J. Sound & Vibration* **197** (1), 17-44.
- Duncan, J. H. and Zhang, S. G. 1993 On the interaction of a collapsing cavity and a compliant wall. *J. Fluid Mech.* **226**, 401-423.
- Feng, Z. C. and Leal, L.G. 1997 Nonlinear bubble dynamics. *Ann Rev Fluid Mech.* **29** 201–43.

- Fuster, D., Dopazo, C. and Hauke, G. 2011 Liquid compressibility effects during the collapse of a single cavitating bubble. *J. Acoust. Soc. Am.*, 129(1), 122-31.
- Fustera, D. and Montel, F. 2015 Mass transfer effects on linear wave propagation in diluted bubbly liquids. *J. Fluid Mech.* 779, 598- 621.
- Geers, T. L. and Zhang, P. 1994 Doubly asymptotic approximations for submerged structures with internal fluid volumes. *J. Appl. Mech.* **61**, 893–906.
- Geers, T. L. and Hunter, K. S. 2002 An integrated wave-effects model for an underwater explosion bubble. *J. Acoust. Soc. Am.* 111, 1584–1601.
- Geers, T. L., Lagumbay, R. S. and Vasilyev, O. V. 2012 Acoustic-wave effects in violent bubble collapse. *J. Appl. Phys.* **112**, 054910.
- Gaitan, D. F., Crum, L. A., Church, C. C. & Roy, R. A. 1992 Sonoluminescence and bubble dynamics for a single, stable, cavitation bubble. *J. Acoust. Soc. Am.* 91, 3166-3183.
- Gomph, B., Günther, R., Nick, G., Pecha, R. & Eisenmenger 1997 Resolving sonoluminescence pulse width with time-correlated single photon counting. *Phys. Rev. Lett.* 79, 1405-1408.
- Hsiao, C.-T., Jayaprakash, A., Kapahi, A., Choi, J.-K., and Chahine, G.L. 2014 Modeling of Material Pitting from Cavitation Bubble Collapse. *J. Fluid Mech.*, 755, 142-175.
- Hsiao, C. T., Jayaprakash, A., Kapahi, A., Choi, J.-K. and Chahine, G. L. 2014 Modelling of material pitting from cavitation bubble collapse. *J. Fluid Mech.* 755, 142- 175.
- Hiller, R. A., Putterman, S. J. & Weninger, K. R. 1998 Time-resolved spectra of sonoluminescence. *Phys. Rev. Lett.* 80, 1090-1093.
- Hiller, R., Putterman, S. J. & Barber, B. P. 1992 Spectrum of synchronous picosecond sonoluminescence. *Phys. Rev. Lett.* 69, 1182-1184.
- Hilgenfeldt, S., Brenner, M. P., Grossman, S and Lohse, D. J. 1998 Analysis of Rayleigh-Plesset dynamics for sonoluminescing bubbles. *Fluid Mech.* 365, 171 - 204.
- Hilgenfeldt, S., Grossmann, S. & Lohse, D. 1999 A simple explanation of light emission in sonoluminescence. *Nature* 398, 402–405.
- Hung, C. F. and Hwangfu, J. J. 2010 Experimental study of the behavior of mini-charge underwater explosion bubbles near different boundaries. *J. Fluid Mech.* **651**, 55-80.
- Iloreta J. I., Fung, N. M. and Szeri A. J. 2008 Dynamics of bubbles near a rigid surface subjected to a lithotripter shock wave: I. Consequences of interference between incident and reflected waves *J. Fluid Mech.* **616**, 43–61
- Jayaprakash, A. Chao-Tsung, H. and Chahine, G. 2010 Numerical and experimental study of the interaction of a spark-generated bubble and a vertical wall. *J. Fluids Engineering* **134** (3), 031301-1
- Jayaprakash, A., Singh, S. and Chahine, G. 2011 Experimental and Numerical Investigation of Single Bubble Dynamics in a Two-Phase Bubbly Medium. *J. Fluids Engineering* **133**, 121305.
- Johnsen, E. and Colonius, T. 2006 Implementation of WENO schemes in compressible multicomponent flow problems. *J. Comput. Phys.*, 219(2), 715–732.
- Johnsen, E. & Colonius, T. 2008 Shock-induced collapse of a gas bubble in shockwave lithotripsy. *J. Acoust. Soc. Am.* 124, 2011–2020.
- Johnsen, E. and Colonius, T. 2009 Numerical simulations of non-spherical bubble collapse. *J. Fluid Mech.* 629, 231–262.
- Keller, J. B. and Kolodner, I. I. 1956 Damping of underwater explosion bubble oscillations. *J. Applied Phys.* **27** (10), 1152-1161.
- Keller, J. B. and Miksis, M. 1980 Bubble oscillations of large amplitude. *J. Acoust. Soc. Am.* **68** 628–33.
- Klaseboer, E., Fong, S. W., Turangan, C. K., Khoo, B. C., Szeri, A. J., Calvisi, M. L., Sankin, G. N. and Zhong, P. 2007 Interaction of lithotripter shockwaves with single inertial cavitation bubbles *J. Fluid Mech.* **593**, 33–56

- Klaseboer, E., Hung, K. C., Wang, C., Wang, C. W., Khoo, B. C., Boyce, P., Debono, S. and Charlier, H. 2005 Experimental and numerical investigation of the dynamics of an underwater explosion bubble near a resilient/ rigid structure. *J. Fluid Mech.* **537**, 387–413.
- Lauterborn, W. and Bolle, H. 1975 Experimental investigations of cavitation-bubble collapse in the neighbourhood of a solid boundary *J. Fluid Mech.* **72**, 391–9.
- Lauterborn, W. and Kurz, T. 2010 Physics of bubble oscillations. *Rep. Prog. Phys.* **73**, 10650.
- Lauterborn, W. and Ohl, C. D. 1997 Cavitation bubble dynamics. *Ultrasonics Sonochem.* **4**, 65–75.
- Lauterborn, W. and Vogel, A. 2013 Shock wave emission by laser generated bubbles. In *Bubble Dynamics & Shock Waves* (ed. C.F. Delale), 67–103. Springer-Verlag Berlin Heidelberg.
- Lee, M., Klaseboer, E. and Khoo B. C. 2007 On the boundary integral method for the rebounding bubble. *J. Fluid Mech.* **570**, 407–429.
- Lezzi, A. and Prosperetti, A. 1987 Bubble dynamics in a compressible liquid. Part. 2. Second-order theory. *J. Fluid Mech.* **185**, 289–321.
- Leslie, T. A and Kennedy, J. E. 2006 High-intensity focused ultrasound principles, current uses, and potential for the future. *Ultrasound Quart* **22**, 263–272.
- Leighton, T. 1994 *The Acoustic Bubble*. Academic Press, London.
- Lindau, O. and Lauterborn, W. 2003 Cinematographic observation of the collapse and rebound of a laser-produced cavitation bubble near a wall *J. Fluid Mech.* **479**, 327–48
- Lohse, D. 2005 Cavitation hots up. *Nature*, 434, 33–34.
- Lundgren, T. S. and Mansour, N. N. (1991) Vortex ring bubbles. *J. Fluid Mech.* **72**, 391–399.
- Marmottant, P. and Hilgenfeldt, S. 2003 Controlled vesicle deformation and lysis by single oscillating bubbles. *Nature* 423, 153–156.
- Naud'e, C. F. and Ellis, A. T. 1961 On the mechanism of cavitation damage by non hemispherical cavities collapsing in contact with a solid boundary *Trans. ASME D: J. Basic Eng.* **83** 648–56
- Pedley, T. J. 1968 The toroidal bubble. *J. Fluid Mech.* **32**, 97 – 112.
- Pearson, A., Blake, J. R. and Otto, S. R. 2004 Jets in bubbles. *J. Eng. Math.* **48** (3-4), 391–412.
- Philipp, A. and Lauterborn, W. 1998 Cavitation erosion by single laser-produced bubbles. *J. Fluid Mech.* **361**, 75–116.
- Plesset, M. S. and Chapman, R. B. 1971 Collapse of an initially spherical vapour cavity in the neighbourhood of a solid boundary. *J. Fluid Mech.* **47**, 283–290.
- Plesset, M. S. and Prosperetti, A. 1977 Bubble dynamics and cavitation. *Ann. Rev. Fluid Mech.* **9**. 145–185.
- Prosperetti, A. and Lezzi, A. 1986 Bubble dynamics in a compressible liquid. Part. 1. First-order theory. *J. Fluid Mech.* **168**, 457–478.
- Ohl, C. D., Arora, M., Ikink, R., de Jong, N., Versluis, M., Delius M. & Lohse, D. 2006 Sonoporation from jetting cavitation bubbles. *Biophys. J.* **91**, 4285–4295.
- Rayleigh, Lord 1917 On the pressure developed in a liquid during the collapse of a spherical cavity. *Phil. Mag.* **34**, 94–98.
- Roberts, W. W., Hall T. L., Ives, K., Wolf, J. S., Fowlkes, J. B. and Cain, C. A. 2006 Pulsed cavitation ultrasound: a noninvasive technology for controlled tissue ablation (histotripsy) in the rabbit kidney. *J. Urol.* **175**, 734–738.
- Rogers, J. C. W., Szymczawk, W. G., Bergera, A. E. & Soloman, J. M. 1990 Numerical solution of hydrodynamic free boundary problems. *Zntl. Series Numer. Maths* **95**, 241–266.
- Shima, A., Takayama, K., Tomita, Y. and Miura, N. 1981 An experimental study on effects of a solid wall on the motion of bubbles and shock waves in bubble collapse. *Acustica* **48**, 293–301.
- Suslick, K. S. 1990 Sonochemistry. *Science* **247**, 1439–1445.
- Suslick, K. S. & Crum, L. A. 1997 in *Encyclopedia of Acoustics* (ed. Crocker, M. J.) 271–282 Wiley-Interscience, New York).

- Szeri, A. J., Storey, B. D., Pearson, A. and Blake, J. R. 2003 Heat and mass transfer during the violent collapse of nonspherical bubbles. *Phys. Fluids* **15**, 2576–2586.
- Szymczawk, W. G., Rogers, J. C. W., Soloman, J. M. & Bergera, A. E. 1993 A numerical algorithm. for hydrodynamic free boundary problems. *J. Comput. Phys.* **106**, 3 19-336.
- Taylor, G. I. 1942 Vertical motion of a spherical bubble and the pressure surrounding it. In *Underwater Explosion Research*, 2, 131–144, Office of Naval Research, Washington, DC.
- Terashima, H. and Tryggvason, G. 2009 A front-tracking/ghost-fluid method for fluid interfaces in compressible flows. *J. Comput. Phys.*, **228** (11), 4012-4037.
- Tinguely, M., Obreschkow, D., Kobel, P., Dorsaz, N. de Bosset, A. and Farhat M. 2012 Energy partition at the collapse of spherical cavitation bubbles. *Phys. Rev. E* **86**, 046315.
- Tomita, Y. and Shima, A. 1986 Mechanisms of impulsive pressure generation and damage pit formation by bubble collapse. *J. Fluid Mech.* **169**, 535–564.
- Turangan, C. K., Jamaluddin, A. R., Ball, G. J. & Leighton, T. G. 2008 Free-Lagrange simulations of the expansion and jetting collapse of air bubbles in water. *J. Fluid Mech.* **598**, 1–25.
- Vogel, A., Lauterborn, W. and Timm, R. 1989 Optical and acoustic investigations of the dynamics of laser-produced cavitation bubbles near a solid boundary. *J. Fluid Mech.* **206**, 299–338.
- Vogel, A., Schweiger, P., Frieser, A., Asiyu, M. and Birngruber, R. 1990 Intraocular Nd:YAG laser surgery: damage mechanism, damage range and reduction of collateral effects. *IEEE J. Quant. Electr.* **26**, 2240-2260.
- Wang, C. and Khoo, B. C. 2004 An indirect boundary element method for three dimensional explosion bubbles,” *J. of Comput. Phy.* **194**(2), 451–480.
- Wang, Q. X. 1998 The numerical analyses of the evolution of a gas bubble near an inclined wall. *Theoret. & Comput. Fluid Dyn.* **12**, 29-51.
- Wang, Q. X. 2004 Numerical modelling of violent bubble motion. *Phys. Fluids* **16** (5), 1610-1619.
- Wang, Q. X. 2013 Underwater explosion bubble dynamics in a compressible liquid. *Phys. Fluids* **25**, 072104.
- Wang, Q. X. 2014 Multi-oscillations of a bubble in a compressible liquid near a rigid boundary, *J. Fluid Mech.* **745**, 509-536.
- Wang, Q. X. and Blake, J. R. 2010 Nonspherical bubble dynamics in a compressible liquid. Part 1. Travelling acoustic wave. *J. Fluid Mech.* **659**, 191-224.
- Wang, Q. X. and Blake J. R. 2011 Nonspherical bubble dynamics in a compressible liquid. Part 2. Acoustic standing wave. *J. Fluid Mech.* **679**, 559-581.
- Wang, Q.X. Liu, W.K., Zhang A. and Sui, Y 2015 Bubble dynamics in very close to a rigid boundary. *Interface Focus*, **5**(5), 20150048. DOI: 10.1098/rsfs.2015.0048.
- Wang, Q. X. and Manmi, K. 2014 Microbubble dynamics near a wall subjected to a travelling acoustic wave. *Phys. Fluids* **26**, 032104.
- Wang, Q.X., Manmi, K., Liu, K.K. 2015 Cell mechanics in biomedical cavitation. *Interface Focus*, **5**(5) 20150018. DOI: 10.1098/rsfs.2015.0018.
- Wang, Q. X., Yeo, K. S., Khoo, B. C. and Lam, K. Y. 1996a Nonlinear interaction between gas bubble and free surface. *Computers & Fluids* **25** (7), 607.
- Wang, Q. X., Yeo, K. S., Khoo, B. C. and Lam, K. Y. 1996b Strong interaction between buoyancy bubble and free surface. *Theor. Comput. Fluid Dyn.* **8**, 73.
- Wang, Q. X., Yeo, K. S., Khoo, B. C. and Lam, K. Y. 2005 Vortex ring modelling for toroidal bubbles. *Theoret. & Comput. Fluid Dyn.* **19** (5), 303-317.
- Wardlaw A. Jr., Luton J.A. 2000 Fluid-structure interaction for close-in explosions. *Shock and Vibration Journal* **7**, 265-275.
- Wardlaw A. B., Luton J. A., Renzi J. R., Kiddy K. C., McKeown R.M. 2003 The Gemini Euler solver for the coupled simulation of underwater explosions. NSWCIHD/IHTR-2500.

- Wardlaw A. Jr., Luton J.A., Renzi J.J., Kiddy K. 2003 Fluid-structure coupling methodology for undersea weapons. *Fluid Structure Interaction II*, WIT Press, 251–263.
- Van Dyke, M. D. 1975 *Perturbation Methods in Fluid Mechanics*. 2nd Edition, The Parabolic Press, Stanford, California.
- Yang, Y. X. Wang, Q. X. and Keat, T. S. 2013 Dynamic features of a laser-induced cavitation bubble near a solid boundary. *Ultrasonics Sonochemistry* 01. DOI:10.1016.
- Young, F. R. 1989 *Cavitation*. McGraw-Hill.
- Zhang, A.M., Cui, P., Cui, J., Wang, Q.X. 2015 Experimental study on bubble dynamics subject to buoyancy. *J. Fluid Mech.*, 776, 137-160.
- Zhang, S. G. and Duncan, J. H. 1994 On the nonspherical collapse and rebound of a cavitation bubble. *Phys. Fluids* **6** (7), 2352–2362.
- Zhang, S. G., Duncan, J. H., and Chahine G. L. 1993 The final stage of the collapse of a cavitation bubble near a rigid wall. *J. Fluid Mech.* **257** 147-181.
- Zhang, Y. and Li, S. C. 2014. Mass transfer during radial oscillations of gas bubbles in viscoelastic mediums under acoustic excitation. *Int. J. Heat Mass Transfer*, 69, 106-116.
- Zhang, Y. L., Yeo, K. S. Khoo, B. C. and Wang, C. 2001 3D jet impact and toroidal bubbles. *J. Comput. Phys.* 166 (2), 336–360.